Οι Επιμήκεις Νανοΐνες σε παροδικά δίκτυα πολυμερών όπως μελετήθηκαν με τη φασματοσκοπία συσχέτισης φωτονίων

Αικατερίνη Α. Ρουσάκη

Μεταπτυχιακή Εργασία κατατεθειμένη στο
Τμήμα Χημείας του
Πανεπιστημίου Κρήτης

Ηράκλειο, Ιούλιος 2004

Long Nanofibers in transient polymer networks as studied by photon correlation spectroscopy

Aikaterini A. Rousaki

A Master submitted to the
Chemistry Department,
University of Crete

Heraklion, July 2004

Acknowledgements

I need to thank the people that have helped and encouraged me throughout this work. Especially I would like to give credit to:

My master advisor, Prof. George Fytas, for his assistance and guidance until the very last moment, as well as for stimulating my interest for research.

Dr Benoit Loppinet, for his continuous interest for my work, his guidance and assistance from my first steps until the end of my work.

In addition, I wish to thank all my colleagues in the laboratory for their help and support.

Finally, I thank my family for their moral support and encouragement.

Aikaterini Rousaki

Contents

Περίληψη

Η χημεία διμερών πολυμερών επιτρέπει την παραγωγή των σωματιδίων με σχεδιασμένη persistent μορφή. Ειδικά τα μακριά κυλινδρικά σωματίδια μπορούν να ληφθούν με τη διασύνδεση ενός πολυισοπρενικού κυλίνδρου με αλυσίδες πολυστυρενίου (Μοριακό Βάρος= 7k) διαμορφώνοντας το κάλυμμα. Η υπερμοριακή δομή, με την πυρηνική διάμετρο d_{PI}= 26,6nm και μήκος κυλίνδρου L_W=1930nm μπορεί να απομονωθεί. Ένα τέτοιο δείγμα ήταν συντεθειμένο και χαρακτηρισμένο από το εργαστήριο του καθ. G. Liu στο Κάλγκαρι δεδομένου ότι το πρόδρομο διμερές συν-πολυμερές είναι το πολυστυρένιο-β-πολυισοπρένιο. Εμείς ονομάζουμε το συσσωμάτωμα που λαμβάνουμε ως αποτέλεσμα PS-b-PI νανοΐνα. Είναι διμερής συμπολυμερής ίνα αποτελούμενη από τον συνδεδεμένο κυλινδρικό πυρήνα φτιαγμένο από ένα πολυμερές (πολυισοπρένιο) και δεμένες στην επιφάνεια αλυσίδες φτιαγμένες από ένα άλλο πολυμερές (πολυστυρένιο).

Χαρακτηρίζουμε τις νανοΐνες σε αραιά διαλύματα σε ισορροπία με στατικά και δυναμικά πειράματα σκέδασης φωτός. Τα αραιά στατικά πειράματα σκέδασης φωτός έδωσαν ικανοποιητικά αποτελέσματα για το μέγεθος R_c και το μοριακό βάρος ανά μονάδα μήκους M_u. Λάβαμε επίσης μία αρκετά καλή προσέγγιση του persistent μήκους l_p και επιβεβαιώσαμε ένα σχήμα με γενική μορφή ράβδου από το προφίλ της σκεδαζόμενης έντασης. Τα δυναμικά πειράματα σκέδασης φωτός έδωσαν μια μάλλον χαμηλή τιμής υδροδυναμική ακτίνα συμβατή με το ανισοτροπικό σχήμα των νανοϊνών.

Προκειμένου να αποκτηθεί μια εικόνα της εσωτερικής δομής και της διάχυσης αυτών των μακριών ινών σε ένα χημικά ίδιο δίκτυο ομοπολυμερών πολυστυρένιο που απεικονίζει την προσαρμογή τους ως υλικά πληρώσεως, έχουμε μελετήσει τη φυσική κατάσταση αυτών των ινών σε διάλυμα πολυστυρένιο για δύο μοριακά βάρη (MB_1=22.2kDa και MB_2=1.200kDa). Χρησιμοποιώντας τη φασματοσκοπία συσχετισμού φωτονίων δύο διαδικασίες παρατηρούνται σαφώς και επιλύονται αδιαμφισβήτητα. Αυτές αποδόθηκαν έπειτα στο ομοπολυμερές και τις νανοΐνες λόγω της ευρέως διαφορετικής έμφυτης δυναμικής των συστατικών αυτού του μοριακού συμπλέγματος. Σε επαρκώς χαμηλές συγκεντρώσεις πολυστυρενίου η συμπεριφορά ενός μόνο μορίου παρατηρείται, ενώ για τις συγκεντρώσεις επάνω από τη συγκέντρωση επικάλυψης πολυστυρενίου C*, όταν διαμορφώνεται ένα παροδικό δίκτυο, οι νανοΐνες τείνουν να συναθροιστούν. Αυτό βεβαιώθηκε σαφώς με την αύξηση έντασης και την επιβράδυνση της διάχυσης νανοϊνών. Οι αλληλεπιδράσεις που οδηγούν στη συνάθροιση προκύπτουν πιθανώς από μια μη ισορροπημένη ωσμωτική πίεση λόγω του αποκλειόμενου όγκου αποβολή των πολυμερών σωμάτων από την περιοχή μεταξύ των μορίων. Ένας μηχανισμός μείωσης (depletion) επάγει τη συνάθροιση στις συγκεντρώσεις μεγαλύτερες από C* και στο χαμηλό και στο υψηλό μοριακού ψηλού βάρους πολυστυρένιο σε περιπτώσεις καλού διαλύτη.

Summary

Diblock copolymer chemistry allows the production of particles with designed persistent shape. In particular long cylindrical particles can be obtained by crosslinking a polyisoprene cylinder with polystyrene chains (M_w=7k) forming the coat. The supramolecular structure, with core diameter d_{PI}=26.6nm and cylinder length L_w=1930nm can be isolated. Such a sample was synthesized and characterized from the laboratory of Prof. G. Liu in Calgary since the precursor diblock copolymer is the polystyrene-b-polyisoprene. We call the resulted assembly the PS-b-PI nanofiber. It is a diblock copolymer nanofiber consisting of crosslinked cylindrical core made of one block (polyisoprene) and surface anchored chains made of another block (polystyrene).

We characterize the nanofibers in dilute equilibrated solutions with static and dynamic light scattering experiments. Dilute static light scattering experiments gave satisfactory results on size R_c and molecular weight per unit length M_u. We also obtained a quite good approximation of the persistent length l_p, and verified a rod like overall shape from the profile of the scattering intensity. Dynamic light scattering experiments yielded a rather low value for the hydrodynamic radius compatible with the anisotropic shape of the nanofibers.

In order to get an insight of the structure and diffusion of this long fibers in a chemically identical network of polystyrene homopolymers reflecting their adaptation as fillers, we have studied the physical state of these fibers in polystyrene solution for two molecular weights (M_{w1}=22.2kDa and M_{w2}=1.200kDa). Utilizing photon correlation spectroscopy two processes are clearly observed and unambiguously resolved. These were then attributed to the homopolymer and the nanofiber due to the vastly different inherent dynamics of the components of this molecular composite. At sufficienly low polystyrene concentrations a single particle's behavior is observed, whereas for concentrations above the overlap polystyrene concentration C*, when a transient network is formed, nanofibers tend to aggregate. This was clearly witnessed by the intensity increase and the slowing down of the nanofibers diffusion. The interactions leading to the aggregation probably arise from an unbalanced osmotic pressure due to the excluded volume driven expulsion of polymers from the region between the particles. A depletion mechanism induces aggregation in concentrations greater than C*in both the low and the high molecular weight polystyrene in a good solvent cases.

I. Introduction

I-1. Diblock for advanced polymers

It is well established that microstructured materials may be industrially prepared, but as the demand for smaller and smaller feature sizes always impose to lower the limits, further steps towards miniaturization have been raised in the last decade, focusing on different and more suitable strategies. Many methods for the fabrication of nanomaterials have been proposed, mainly to meet the demand of the microelectronic industries, ranging from milling techniques to non-traditional photolithographic and chemical methods, with a strong prevalence of methods based on template synthesis[1].

However, their main weakness still remains in the difficult and poor control of the final morphology of the produced nanostructures. In such a sense polymers represent ideal nanoscale tools[2], not only due to their intrinsic dimensions, ease of synthesis and processing, strict control of architecture and chemical functionality, but also because of their peculiar mesophase separation both in bulk and in solution particularly in the case of block copolymers[3]. Block copolymers may be considered as two or more chemically homogeneous polymer fragments, i.e., homopolymer chains, joined together by covalent bonds to form more complex macromolecules such as linear di-, tri-, or multiblock copolymers, and nonlinear architectures such as multiarm, starblock, or graft copolymers (Figure I-1).

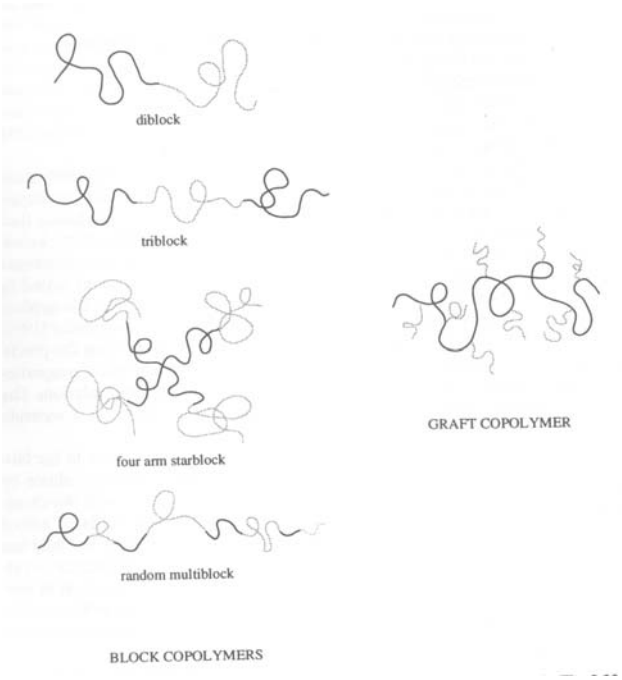

Figure I-1: The architecture of copolymers can be controlled by a synthesis procedure, and it is possible to prepare diblock, triblock, multiblock, starblock and graft copolymers.

In the frequent case of immiscibility among the constituent polymers, the competing thermodynamic effects give rise to different kind of self-assembled

morphologies, depending both in structural and dimensional terms on composition, segmental interaction, and molecular weights, and having periodicity suitable for application in nanotechnology[4].

The existence of some morphologies can be theoretically predicted. More recent efforts have focused on ordered structures obtained from block copolymers having both rigid and flexible segments. Interest is also given on triblock and even tetrablock copolymers with the observation of a series of novel and unconventional morphologies such as zig-zag, core-shell double gyroid, spheres or rods between lamellae, helices around cylinders and hexagonal double or triple coaxial cylinder structures. A few of these morphologies, the ones most frequently used for nanofabrication, are illustrated schematically in figure I-2.

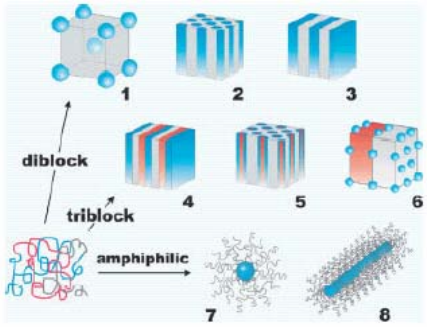

Figure I-2: Sketches of equilibrium morphologies from block copolymer self assembly, among the most frequently used for nanofabrication. For diblock copolymers in bulk: body centered cubic packed spheres (1), hexagonically ordered cylinders (2), lamellae (3). For triblock copolymers: lamellae (4), hexagonial coaxial cylinders (5), spheres betwwen lamellae (6). For amphiphilic block copolymers in solution: spherical micelles (7), and cylindrical micelles (8). The figure is from M.Lazzari, M.Arturo Lopez-Quintela Adv. Mater. 15, 1583, 2003.

Depending on the structure of the "head" and "tail" a small molecule surfactant in a solvent may form micelles of different shapes including spheres, cylinders, discs and vesicles. Diblock-copolymers also form micelles of different shapes. In bulk, the two blocks of a diblock copolymer segregate to form different domains packed with long range order. The domain structure for the minor component can be spherical, cylindrical, gyroidal, or lamellar depending on the volume fraction of the minor component.

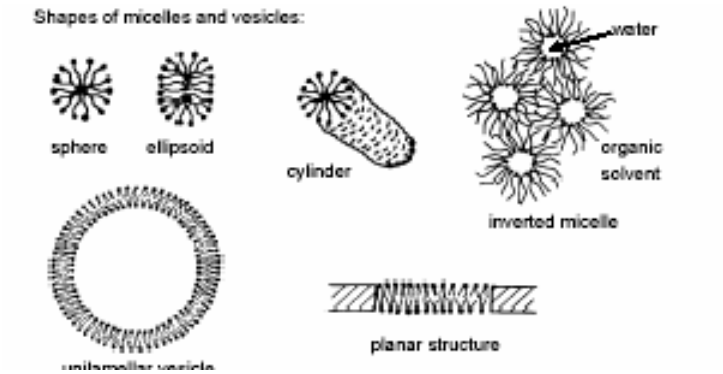

Figure I-3: Micelles of different kinds are formed depending on the conditions.

Micellization occurs when block copolymer chains associate into, often spherical, micelles in dilute solution in a selective solvent. The core of the micelle is formed by the insoluble or poorly solvated block, whilst the corona contains the selectively solvated block. Such micelles are illustrated in figure I-3. At a fixed temperature, micellization occurs on increasing concentration at the critical micelle concentration.

The formation of rodlike micelles is commonly favored at higher concentrations. When copolymer chains become maximally swollen by solvent, spherical micelles can no longer grow, and elongated micelles tend to form. The phase behavior of block copolymers consisting of flexible polymer coils is remarkably rich. If one of the blocks is rigid (nanofibers case), the copolymer would be expected to exhibit even more complex phase behavior. Diblock copolymers consisting of a rigid block attached to a coiled block are termed rod-coil copolymers.

At even higher concentration we have formation of lamellae.

Another way to form various shapes of block copolymers except micellarization is to take advantage of their phase separation ability.

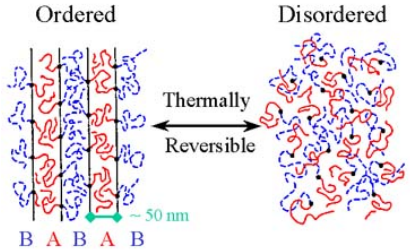

Figure I-4: Free mixing of blocks at sufficiently high temperature or when sufficiently diluted.

The blocks can sometimes intermix freely at sufficiently high temperature, or when sufficiently diluted with solvent, generating the "disordered" structure shown above (Figure I-4). However, it is common for the blocks to spontaneously self-assemble ("order", as shown above) into a diversity of mesophases, with the size scale governed by the chain dimensions. In the mesophases, dissimilar blocks exist in distinct "microdomains" which are highly enriched in blocks of the same type, sometimes to the point of being essentially pure. The covalent bonds linking the dissimilar blocks are thus localized to the vicinity of the microdomain interfaces. While the cartoon above illustrates the case where the A and B blocks are of comparable lengths, the block ratio is easily varied during polymer synthesis to alter the mesophase structure. The known equilibrium mesophases for diblock copolymers (spheres, cylinders, gyroid, and lamellae) are shown in the phase diagram (figure I-5).

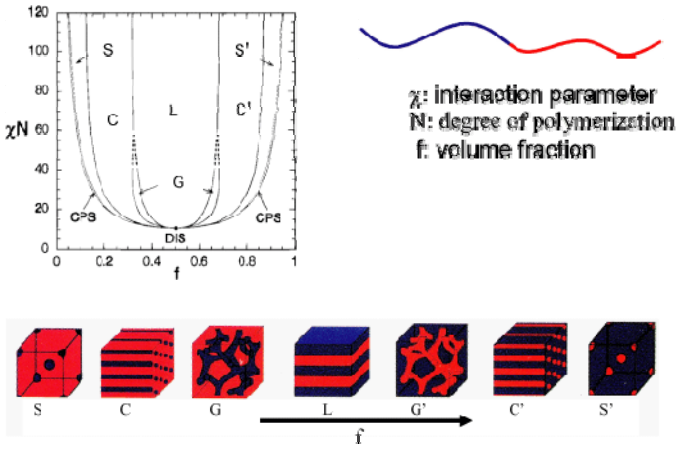

Figure I-5: Schematic diblock copolymer phase diagram: f = volume fraction of one block, χ = Flory interaction parameter, N = diblock degree of polymerization. Known equilibrium mesophases are S(pheres), C(ylinders), G(yroid), and L(amellae), as well as the disordered (DIS, homogeneous) at small interblock segregation strength (χN). (Matsen et al Phys.Rev.Lett 1994, 72, 2660)

The phase diagram depicts the regions occupied by the different morphologies as a function of the interaction parameter χ, the molecular weight N, and the volume fraction *f*. The x-axis shows increasing fraction of the blue block with respect to the red block, *f*, and on the y-axis is plotted the product of cN, which is inversely proportional to temperature; thus, at high temperature entropy dominates and the polymer falls into the disordered state. The resulting morphologies are described as spheres (S), cylinders (C), gyroid (G), lamellae (L), and their respective inverses (represented by S', C', and G').

Fundamental studies on AB block copolymer thermodynamics rely on the preparation of monodispersed materials with well-defined molecular weights (MWs) and block volume fractions (*f*). This is typically accomplished through a living polymerization technique by sequential monomer addition. Due to the absence of chain transfer and chain termination, living polymerizations allow for precise definition of M_w and *f*.

I-2. Nanofibers are big semiflexible fibers

The chemist's imagination can take advantage of the phase diagram abilities and form various exotic architectures of diblock copolymers. The nanofiber supramolecular structures that we cope with in this thesis can be considered as big rigid fibers with many similarities to semiflexible polymers (figure I-6).

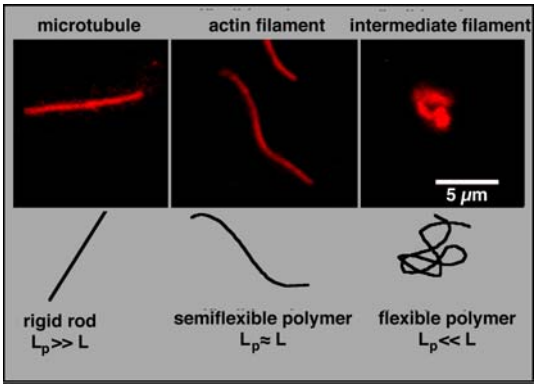

Figure I-6: The size and shape of polymers in the three cases rigid rod, semiflexible polymer and flexible polymer are seen in detail. Rigid rods are persistent molecules with persistent length, which tends to infinity, semiflexible molecules, as the nanofibers, are an intermediate state and flexible polymers have a limiting persistent length.

PS-b-PI nanofibers were prepared by stirring S_2Cl_2-treated PS-b-PI films in THF to separate and disperse the cross-linked PI cylindrical domains. Nanofiber fractions were obtained by combining centrifugation, fractionation and ultrasonication. Their counterparts in a PS-b-PI nanofiber would be the crosslinked PI cylinder and PS chains, respectively. More specifically if we crosslink the parallel to the axis domains of a cylinder (core) with sulfuric bonds we can get the nanofibers, a supramolecular structure.

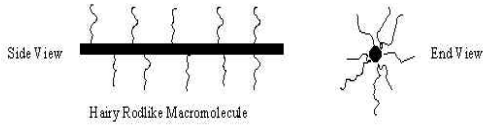

Figure I-7: Macroscopic representation of the nanofiber chain with side and end view.

I-3. Motivation of the present work

Two questions arise: First how will the nanofiber diffuse in a solution of polymers? And second what effective interactions exist between the nanofibers? The nanofibers in contrast to the tiny polystyrene macromolecules dispersed in the toluene solvent have potentials to interact with each other and give oriented structures (nematic, smectic, cholesteric). They can also phase separate if the thermodynamics of the system implies so. Another possibility would be that the system forms intricate supramolecular aggregates. All these possibilities and what really happens will be addressed in the present work. On the other hand the investigation of the diffusional dynamics of the nanofibers embedded in the polymer network might reveal the viscoelastic properties of the latter[5].

In this work we investigate the dynamic and static properties of the semiflexible nanofibers of figure I-7 in polymeric solutions. First we have characterized the sample in dilute solution by obtaining the relevant conformational parameters as the persistent length, the linear mass density and the core radius. The subsequent study of the

nanofibers in chemically similar homopolymers aims at the elucidation of the diffusional motion and/or the importance of depletion effects.

References

1. G.M. Whitesides, J.P. Mathias, C.T. Seto. *Science*, 254, 1312 (1991).
2. H. Li, W.T.S. Huck. *Curr. Opin. Solid. Mater. Sci.*, 6, 3 (2002).
3. N. Hadjichristidis, M. Pitzikalis, S. Pispas, H. Iatrou. *Chem. Rev.*, 101, 3747 (2001).
4. I.W. Hamley. J. Phys.: *Condens. Matter.*, 13, R643 (2001).
5. J.Vander Gucht et al. *Phys. Rev.*, E 67, 051106 (2003) and references herein.

II. Theoretical background

II-1. The regimes of concentration

The overlap threshold c*: A fundamental distinction exists between dilute polymer solutions where the coils are separate and more concentrated solutions where the coils overlap.

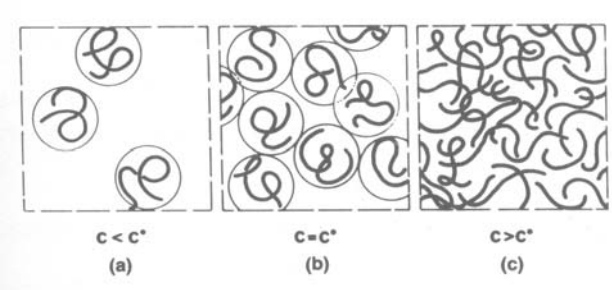

Figure II-1: Schematic representation of macromolecules in the a) dilute, b) overlap, c) semidilute regime[2].

At the overlap threshold (c=c*) the coils begin to be densely packed. Clearly this threshold is not sharp; it is more properly defined as a region of crossover between regimes (a) and (c) (figure II-1).

II-2. Depletion

When the polymer concentration is increased to the point where the polymer coils interpenetrate each other (the semidilute regime) depletion appears.

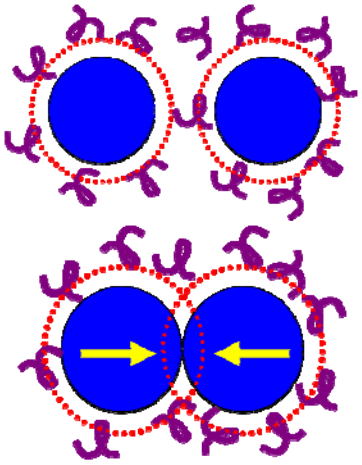

Figure II-2: The Depletion Mechanism. Polymer molecules of radius R_g cannot enter the region between the closely spaced particles of radius R. As a result a net attractive potential is set up by the introduction of polymer into the solution.

There exists a depletion zone around a colloidal particle of thickness R_g, from which the polymer is excluded. When two colloidal particles come together, their depletion zones overlap, and this volume is now accessible to the polymer elsewhere in

the system, increasing the entropy of the polymer. Hence, there is a net attraction between the colloidal particles purely due to entropic reasons, given by

$$\frac{U(r)}{k_B T} = \Pi(c) V_{overlap}(r) \qquad II-1$$

where Π(c) is the osmotic pressure of polymer in solution, and $V_{overlap}$ (r) is the excluded volume of polymer as a function of r, the inter-particle separation. We can determine $V_{overlap}$ by purely geometric considerations.

In our case we do not have spheres to interact through the depletion mechanism but fibers. Both the range and the absolute value of the depletion interaction can increase when rodlike macromolecules are used instead of spherical ones as the depletant[2].

Bollhuis and Frenkel[4] presented a numerical study of the phase diagram of a mixture of spherical and infinitely thin rodlike colloids using simulations and first order perturbation theory.

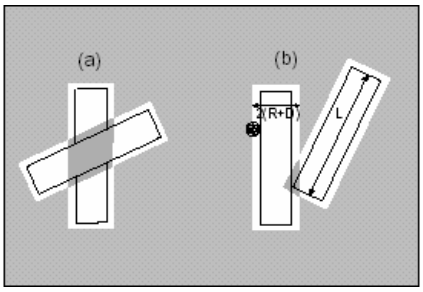

Figure II-3: Each rodlike particle (length *L* and radius *D*) is surrounded by a depletion zone (white). When the excluded-volume shells of a pair of rods overlap, the total volume accessible to the polymer increases. The free volume (dotted area) is increased by the overlap (dark) of depletion zones. The depletion interaction consists of the overlap volume between crossed cylinders (Fig. II-3(a)) and that of the ends of rods (Fig. II-3(b)). When the length *L* of the rod is sufficiently large, the main contribution to the free volume is from the overlap of the crossed cylinders[6].

One of the central problems to describe phase behavior is to calculate the free volume. Warren[6] has calculated the depletion interaction (or free volume) by considering the overlap (Fig. II-3(a)) of crossed cylinders and showed that the depletion interaction is independent of the orientational order parameter of rods. The phase diagrams calculated on the polymer-rod concentration plane show a widening of the biphasic region between a nematic and an isotropic phase at low polymer concentrations. The free volume of the rods has also been estimated using scaled particle theory[7] and simulation[10]. Lekkerkerker *et al*[8]**.** have calculated the free volume based on the scaled particle theory and .found that the free volume is dependent on the orientational order parameter of rods[9]. They found three-phase coexistence such as isotropic-isotropic-nematic and isotropic-nematic-nematic phases.

An alternative theory that accomplished this uses scaled particle free energy (SPTA) of hard rods as a basis to study the influence of attractive interactions on the *I-N*

phase transition [from now on called scaled particle theory with attractions (SPTA)]. The scaled particle expression for hard rods includes third and higher virial coefficients. Therefore it is reasonable to expect that this theory would be more accurate at higher rod and/or polymer concentrations. An additional advantage of the SPTA theory is that it does not assume that the depletion interaction is pairwise additive. Computer simulations have shown that pairwise additivity of the intermolecular potential assumption is not an adequate approximation when the radius of the polymer is larger than the radius of the colloid[10].

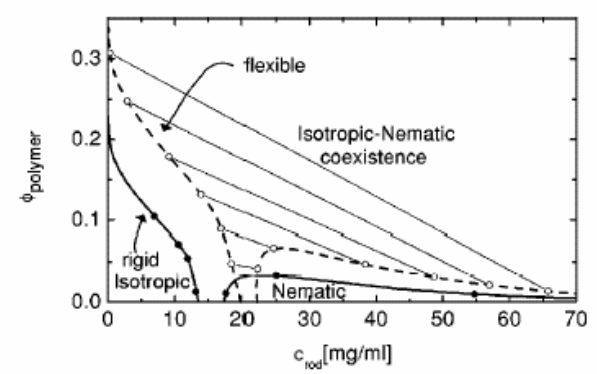

Figure II-4: Phase diagram for rigid and semiflexible rods calculated using the SPTA theory. The boundary between the isotropic- (I) nematic (N) two-phase region and the region where a single phase is stable is indicated by the thick dashed line for semiflexible rods and thick full lines for rigid rods. Tie lines between the coexisting phases are shown by thin lines. For the flexible particle the ratio of the contour length to persistence length is L/P=0.4. The polymer concentration is defined as follows: ϕpolymer=p($4\pi Rg^3$ /3).

Additionally, there have been many studies of depletion driven phenomena, especially phase behavior in model colloids ranging from charged colloids such as polystyrene latex mixed with water soluble polymers, hard particle colloids mixed with polymer, and binary mixtures of spherical colloids. For special geometries microphase separation is observed in mixtures. With binary mixtures of hard spheres this occurs for certain ratios of sphere diameters and for mixtures of rods and spheres microphase separation occurs for certain rod length to sphere diameter ratios.

II-3. Physical Principles of Light Scattering

There are two ways to glean information from scattered laser light. The first method, called Static or Integrated Light Scattering (SLS or ILS), is to observe intraparticle interference patterns of scattered light by measuring the intensity as a function of angle. The second method, called Dynamic Light Scattering (DLS), is to monitor fluctuations in scattered light as a function of time. DLS has a wide range of measurable sizes because it is concerned with the distance ($2\pi/q$) that a particle diffuses in a correlation time.

As for bulk condensed matter in general, analysis of the microscopic structure of polymer systems is mostly carried out by scattering experiments. The general set up of the scattering experiment is indicated schematically in figure II-5.

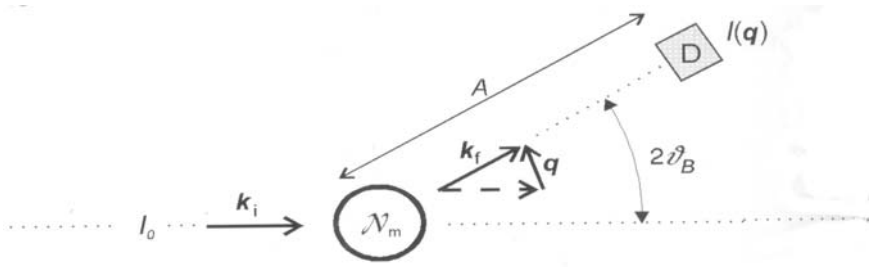

Figure II-5: The general set up of the scattering experiment[1].

We have an incident beam of monochromatic radiation with wavelength λ and intensity I_o. It becomes scattered by a sample and the intensity I of the scattered waves is registered by a detector (D) at a distance A under variation of the direction of observation. Employing the 'scattering vector' q, defined as

$$q=k_f-k_i \qquad II\text{-}2$$

where k_f and k_i denote the wave vectors of the incident and the scattered plane waves, the result of a scattering experiment is usually expressed by giving the 'intensity distribution in q space', I(q). In the majority of scattering experiments on polymers the radiation frequency remains practically unchanged. Then we have

$$\left|k_f\right| \approx \left|k_i\right| = \frac{2\pi}{\lambda} \qquad II-3$$

and $|q|$ is related to the 'Bragg scattering angle' θ_B by

$$\left|q\right| = \frac{4\pi}{\lambda}\sin\partial_B \qquad II-4$$

(θ_B is identical to half of the angle enclosed by k_i and k_f)

In the static light scattering case the fluctuations are not registered and the detector only furnishes the mean value of the scattering intensity, which is dependent only of the angle and not of the time I(q). Static or Integrated light scattering (ILS) techniques offer a sensitive, non-invasive method of measuring particle radii. Firstly, the quantity measured is the total intensity of scattered light, I_s, relative to the intensity of the incident beam, I_o, and the distance, d, from the sample to the detector. Secondly the Rayleigh Ratio is directly related to the true radius of the scattering particle. By fitting the theory of the Rayleigh-Gans-Debye (RGD) approximation to the Rayleigh Ratio measured as a function of the scattering vector, I(q), it is possible to obtain structural properties such as the size and shape of particulates in solution. q, is a function of scattering angle.

The ALV automated goniometer set-up, was employed for the static measurements. The range of angles scanned was 10^o to 150^o and the reference solvent was toluene. By static light scattering we often measure absolute values of molecular weights and thus the absolute value of the scattering intensity is needed.

In infinite dilution conditions, each molecule scatters independently of the other molecules. At the scattering angle θ relative to the incident beam, the scattering intensity of the molecule is I_s. The relative scattering intensity I_s/I_o is defined as the ratio of scattering intensity I_s to the intensity I_o of the incident light. The ratio $R_\theta=I_s/I_o$ is called the Rayleigh ratio.

The expression for the Rayleigh ratio delivers:

$$R_\partial = \left(\frac{4\pi^2 n_1^2 (dn/dc)^2}{N_A \lambda_o^4} \right) CM = K_\partial CM \qquad II-5$$

The Rayleigh ratio of toluene at 90° for wavelength λ=532nm is dependent on temperature:

$$R_\theta = 6.407\ 10^{-6}\ (1+0.0114T)\ cm^{-1} \qquad II\text{-}6$$

For 20°C it values to $R_\theta = 2.782\ 10^{-5}\ cm^{-1}$.

It is calculated from the value given by Bender et al[1].

Scattering experiments at low angles on dilute colloidal systems, polymer solutions included, can be applied for the determination of the molecular weight and the size of colloids or polymers. So we obtain an expression for the structure factor in the limit of low q's.

$$P(q) \approx N\left(1 - \frac{q^2 R_g^2}{3} + \ldots\right) \qquad II-7$$

The equation, often addressed in the literature as 'Guinier's-law, tells us that measurements in the low angle range can be used for a determination of the size of a polymer, as characterized by R_g and the mass, as given by N.

The intensity of light scattered from an array of n particles, relative to scattering at q=0 from a single point particle, is

$$I(q)=nP(q)S(q) \qquad II\text{-}8$$

Where for dilute systems we have

$$S(q)\approx 1 \qquad II\text{-}9$$

And for a sphere of radius R, we have

$$P_1(q) = \left\{ \frac{3}{(qR)^3} [\sin(qR) - qR\cos(qR)] \right\}^2 \qquad II-10$$

An infinitely thin nod shows the high –q asymptotic behavior:

$$P_z(\theta) = \frac{\pi}{qL_w} \qquad II\text{-}11$$

or

$$K_c / \Delta P_\theta /_{c\to 0} = \frac{qL_w}{\pi M_w} = \frac{q}{\pi M_u} \qquad \text{II-12}$$

Thus, the $K_c / \Delta P_\theta /_{c\to 0}$ values at the high q and enable $M_u=M_W/L_w$ evaluation.

The finite cross–section of a nanofiber $P_z(q)$ in the high q region is

$$P_z(q) = \left(\frac{\pi}{qL_w}\right) P_c s(q) \qquad \text{II-13}$$

where $P_c s(q)$, the cross–section scattering function, can be calculated from an expression approximated by Liu et al, by assuming a uniform cross–section for fibers. A rough calculation indicated that $P_c s(q)$ was close to 1 for all q values used.

Einstein and Smoluchowski considered chaotic thermal motion of molecules. A Brownian particle is 'fidgeting' because it is pushed by a crowd of molecules in random directions. In other words, we could say that Brownian particles are themselves engaged in chaotic thermal motion. If we register the Intensity versus time I(q,t) represents the sum of Intensities due to diffusion from a solution comprised from the solvent and the Brownıan particles (macromolecules for example).

$$I(t)_{solution} = I(t)_{polymer} + I(t)_{solvent} \qquad II-14$$

The fluctuation of I(q,t) around it's mean value <I> is due to the random movement of Brown particles in a diffusing volume defined by the experimental geometry. An illustration of the fluctuation I(q,t) is given in figure II-6.

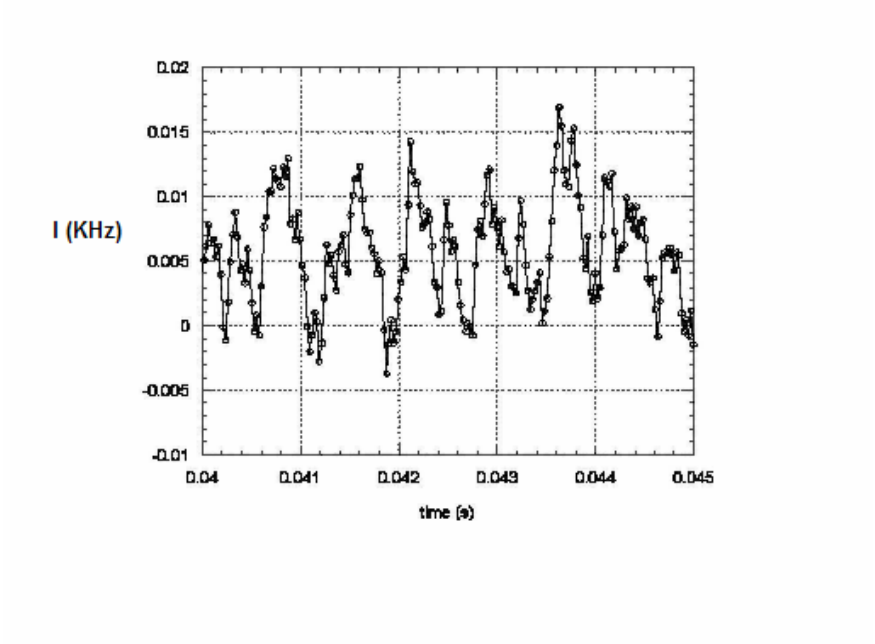

Figure II-6: The Intensity of fluctuations of the Brownian particles.

The hydrodynamic radius is the radius of an equivalent sphere in terms of the dynamic features of a structure. Generally it pertains to the hydrodynamic drag or friction factor, ξ, associated with a particle. For thermal motion such as Brownian motion D is related to kT. The coil is then hydrodynamically a sphere and we can use the Stokes-Einstein relationship for the friction factor, $\xi=6\pi R_h n_{solvent}$. Dynamic light scattering involves measurement of the flickering of scattered laser light from a polymer solution. It is assumed that the flickering is related to thermal motion of the particles in a solution and the Stokes-Einstein relationship, $D=kT/(4\pi R_h n_{solvent})$ (eq. *II-15*), together with an exponential decay in correlations of fluctuations in time, $S(q,t) = K \exp(-2Dq^2t)$, where $S(q,t)$ is the scattered intensity as a function of q and time, t. Where $\Gamma=Dq^2$ 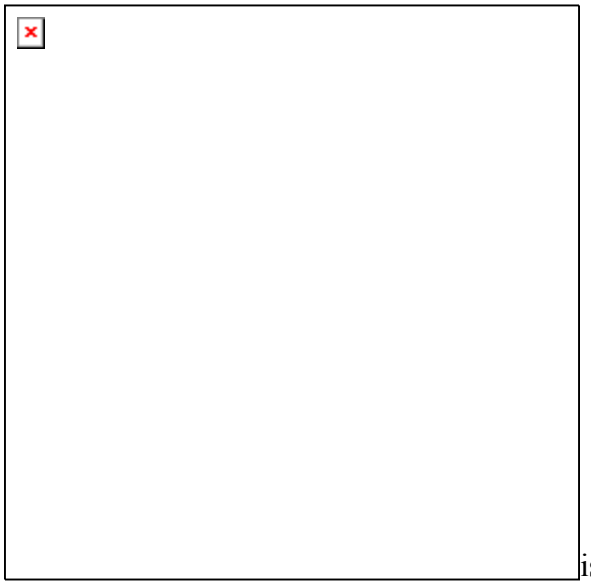 is the decay constant, D 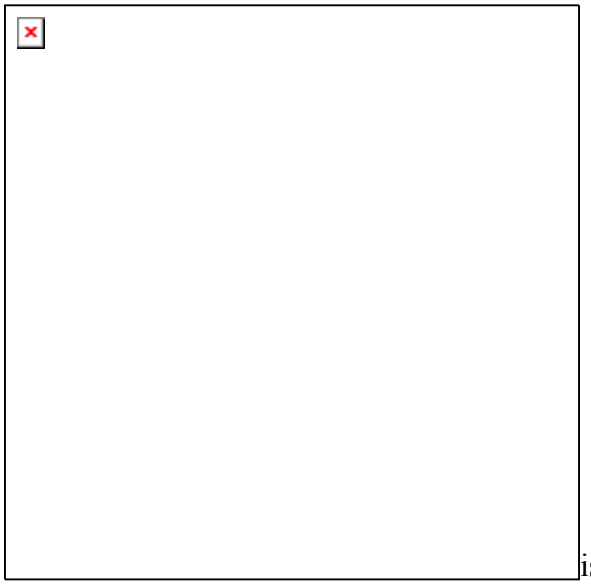 is the diffusion coefficient and q

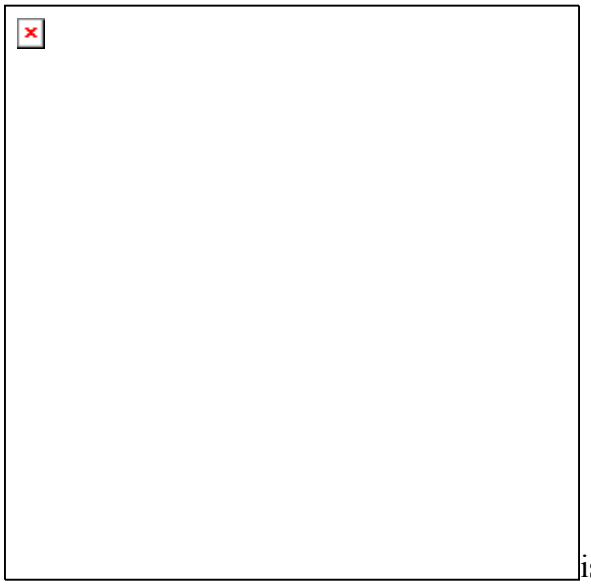
is the magnitude of the scattering vector. Here k 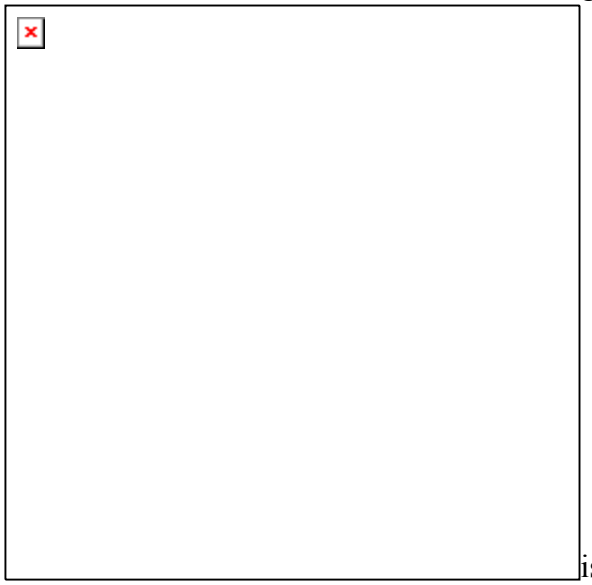
is the Boltzmann constant, T

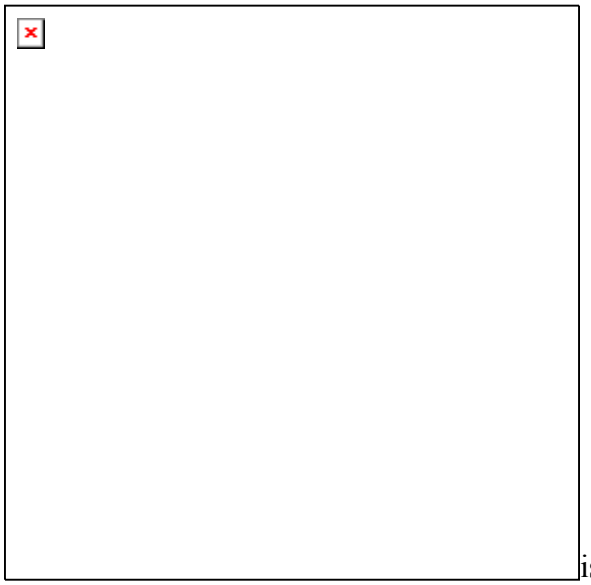
is the temperature , and n
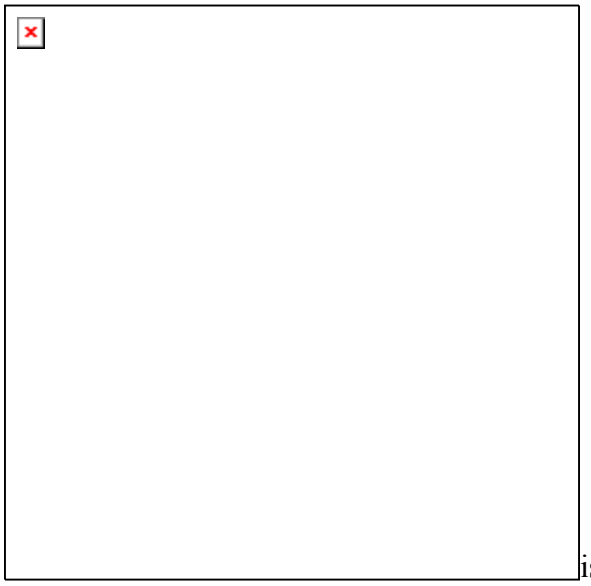
is the viscosity of the suspending liquid.

A system of symmetric top scatterers decays exponentially with a characteristic decay rate $\Gamma_{VH}=q^2D+6D_R$, where D is the translational diffusion coefficient and D_R is the rotational diffusion coefficient. The depolarized Intensity is given from $I_{VH}(q,t) \approx \exp(-\Gamma_{VH}t)$. However, for dense systems such as concentrated solutions or pure liquids, the rotations are no more unrestricted and the neighboring scatterers do not move independently. Then, as in the case of the polarized light scattering, the collective motions of the fluid should be considered.

References

1. G. Stobl. The Physics of Polymers. *Springer* (1996).
2. Pierre-Gilles de Gennes. Scaling concepts in Polymer Physics. *Cornel University Press* (1979).

3. S. Asakura and F. Oosawa. *J. Chem. Phys.*, 22, 1255 (1954).
4. P. Flory. Principles of Polymer Chemistry, Chap. XII. *Cornell University Press*, Ithaca, New York (1971).
5. P. Bolhuis and D.J. Frenkel. *J. Chem. Phys.*, 101, 9869 (1994).
6. A. Matsuyama and T. Kato. *The European Physical Journal*, E6, 15 (2001).
7. P.B. Warren. *J. Phys. I*, 4, 237, (1994).
8. H.N.W. Lekkerkerner, A. Stroobants. *Nuovo Cimento D*, 16, 949 (1994).
9. P.G. Bolhuis, A. Stroobants, D. Frenkel, H.N.W. Lekkerkerker. *J. Chem. Phys.*, 107, 1551(1997).
10. Z. Dogic, K. Purdy, E. Grelet, M. Adams and S. Fraden. *Phys. Rev. E*, 69, 051702 (2004).
11. B.J. Berne, R. Pecora. Dynamic Light Scattering with applications to chemistry, biology and physics. *John Wiley and sons* (1976).

III. Experimental

III-1. Sample

The nanofibers were synthesized in the G. Liu in Calgary. A diblock nanofiber is defined as a cylindrically shaped aggregate of a diblock copolymer. In an isolated nanofiber, one block constitutes the cross-linked core and the other block forms the concentric shell. When dissolved in a good solvent, chains of the shell block would swell and stretch out into the solution phase. Nanofibers were prepared from crosslinking cylindrical micelles formed from a polystyrene–block–polyisoprene sample with 74 styrene and 230 isoprene units in N,N–dimethylacetamide. A PS-b-PI sample has been prepared by anionic polymerization. The diblock formed cylindrical micelles in DMAC. Nanofibers were obtained by reaction of S_2Cl_2 with the cylindrical micelles. The nanofibers were characterized by TEM, LS and viscometry.

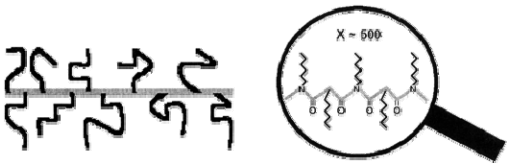

Figure III-1: Diblock copolymer nanofiber consists of a crosslinked cylindrical core made of one block and surface-anchored chains made of another block.

By fine tuning the relative length of a diblock copolymer, one can prepare cylindrical micelles from a diblock in a block–selective solvent Nanofibers are obtained via core crossliking of cylindrical micelles In bulk, block copolymers self-assemble forming various intricate nanometer-sized block segregation patterns. Nanofibers are obtained by crosslinking the minority block and separating the hairy cylinders via solvent dispersion.

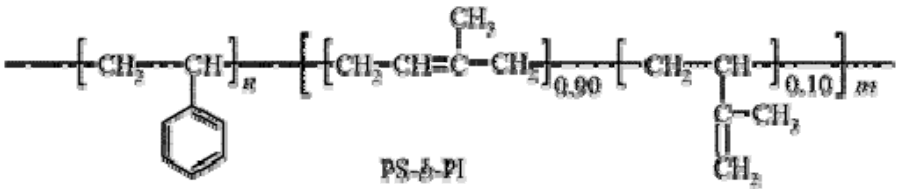

Figure III-2: The chemical formula of the block that the PS-b-PI nanofibers are consisted of.

The use of the crosslinking agent sulfur monochloride, S_2Cl_2, as the limiting agent there would have lead to preferential crosslinking of the PI domains in the surface layers of a film and yielded nanofibers with a range of crosslinking densities.

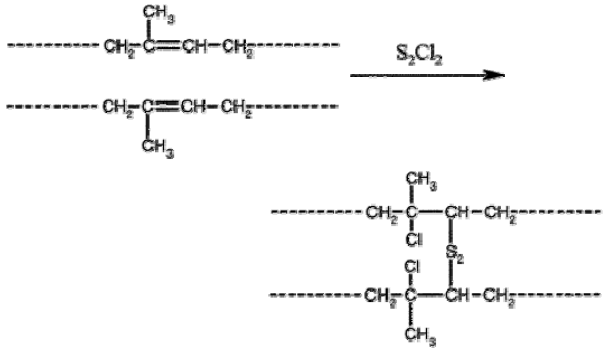

Figure III-3: The cross-linking reaction of the PI cylindrical domains.

Using transmission electron microscopy, light scattering, viscosity measurements and a ^1H NMR spectrum of the nanofibers in $CDCl_3$ the obtained molecular characteristics weight and number averaged lengths L_w, L_N and core radius of the utilized crosslinked nanofibers are listed in Table III-1.

The number–average length, L_N, and weight–average length, L_w were calculated with results shown in Table III-1.

Table III-1

Sample	TEM L_w (nm)	TEM L_N (nm)	TEM d_{PI} (nm)	dn_r/dc (mL/g)	M_w (g/mol)	R_G^*/nm	l_p/nm	M_u g/(mol nm)	SLS L_w^*/nm
X2	1930	1310	26.6±1.7	0.148	$(3.53\pm0.06)\times10^8$	443±1	365±5	2.00×10^5	1770

* obtained from static light scattering study.

III-2. Sample preparation

The samples that were measured were nanofibers in THF and toluene solvent and nanofibers in toluene solvent in polystyrene solution of two molecular weights (22,2kDa) and 1,210kDa).

The change of the solvent was done via continuous evaporation of the THF solvent and addition of the toluene solvent. That procedure lasted approximately one month. We took real care so as not to dry the nanofibers, because the regain of them would last more than six months.

The polystyrene solutions of both the high and low molecular weights were done via dilution of dry polystyrene in the solvent. Then we added a few drops of the nanofibers solution. The intensity was checked so as in all the tubes to have the same concentration of nanofibers. We first measured in dilute polystyrene solution with nanofibers. Then we added some extra polystyrene solution we evaporated the extra toluene until the volume we previously had, we measured the new polystyne concentration maintaining the nanofibers concentration constant and so on.

III-3. Photon Correlation Spectroscopy (PCS)

The dynamic light scattering measurements in the time domain (Photon Correlation Spectroscopy) were done using two different experimental geometries (polarized and depolarized). In figure III-4 we show a schematic of the goniometer set up where we can measure at scattering angles from 10^o to 150^o.

The polarization of the incident and the scattered beam, is determined by two Glan-Thomson (Halle, Berlin) polarizers (P1 and P2) of extinction ratio 10^{-6} and 10^{-7} respectively. In our experiments the incident polarization is always vertical to the scattering plane (V), while the analyzer (P2) in the scattered beam can be rotated, so that, we either measure the vertically (V) or the horizontally (H), polarized part of the scattered radiation. In this way the polarized, $I_{VV}(q)$, and the depolarized, $I_{VH}(q)$, scattered intensities are detected.

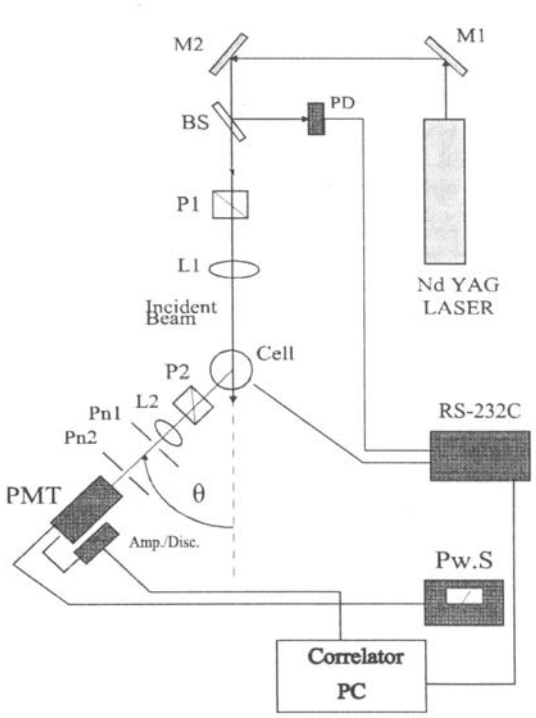

Figure III-4: Schematic representation of the goniometer set up where we can measure at scattering angles from 10^o to 150^o.

The goniometer set-up consists of an automated ALV goniometer which uses as light source an Nd:YAG diode pumped air-cooled laser (Adlas DPY 315 II) with a single mode beam with wavelength of λ=532nm and maximum intensity >100mW. The beam diameter is 0.32 nm (Gaussian beam diameter of TEM_{00} mode) while the power used in our experiments was set to approximately 80mW for stability reasons. The incident beam is focused in the sample with the use of an achromat lens (L1) with F=200mm focal length. Both the intensity and the position of the incident beam are monitored by a set of

four photodiodes (PD). The sample cell, an optical quality glass tube of, is placed in a liquid bath (Cell) which contains an index matching fluid (in our case toluene) to avoid reflections at the sample cell glass. In this way measurements at high (150^o) and especially at low angles (10^o-30^o) are not affected by stray light. The scattered intensity is collected by the detector optics. The temperature of the bath, and consequetly of the sample was regulated by circulation of a thermostated liquid (a mixture of water and glycol was used) with the use of a thermostat. The temperature was measured in the liquid bath by a thermocouple (ALV/Pt-100). The temperature used in the goniometer set up is 20^o C. All the functions of the goniometer were controlled by a PC with the help of the Bus Controller RS-232C. In the goniometer set up we use the ALV-5000/E correlator.

In practice, what is measured in a PCS experiment is the normalized intensity correlation function.

$$g^{(2)}(q,t) = \frac{< I(q,0)I(q,t) >}{< I(q) >^2} = 1 + (f^*)^2[C(q,t)]^2 \qquad III-1$$

The correlator which, an instrument (a electronic board) capable of obtaining the correlation function of an electrical signal. In our experiments we used a ALV-5000/E multiple Tau digital correlator. In it's normal version it uses 288 channels to measure correlation functions over the time range from 10^{-6} to about 10^3 sec.

A theory is needed to calculate the correlation functions of the dielectric (or polarizabiliry) fluctuations of the system and relate them to quantities such as concentration, orientation, size and shape of molecules, as well as the interactions among them. All the dynamic light scattering measurements in this work were carried out under homodyne conditions. The Gaussian approximation was fulfilled in almost all cases.

III-4. Analysis of the correlation functions

Whenever possible, the analysis of the experimental field correlation function C(q,t), was carried out by performing the inverse "Laplace transform" (ILT), using the program CONTIN. The method assumes that C(q,t) is represented by a superposition of exponentials.

$$C(q,t) \equiv ag(q,t) = \int_{-\infty}^{+\infty} L(\ln\tau)\exp(-t/\tau)d(\ln\tau) \qquad III-2$$

which describes a continuous spectrum of relaxation times L(lnτ) which is actually the distribution of relaxation times. L(lnτ) is used to determine the average characteristic relaxation times,τ, from the peak positions of the distribution, as well as the intensity of each relaxation process from the area under the corresponding peak.

In some cases involving relaxation processes which decay faster than single exponential, the ILT analysis is not adequate, and the correlation functions are represented by the Kohlrausch-Williams-Watts (K_{WW}) function:

$$g(q,t) = \exp[(-t/\tau)^{\beta}] \qquad III-3$$

where β is the shape parameter. Normally, $1 \geq \beta \geq 0$, with $\beta=1$ corresponding to a single exponential relaxation mode; the rare case $\beta>1$ is associated with steeper than single exponential decays which physically involves some kind of ballistic motion or turbulence. Moreover, the use of K_{WW} function to fit the correlation function is useful for the estimation of the broadness of the correlation ($1 \geq \beta$) which is an indication of either polydispersity or the existence of more than one relaxation modes.

References

1. X. Yan, G. Liu, H. Li. *Langmuir*, *20*, 4677 (2004).
2. G. Liu, X. Yan, S. Duncan. *Macromolecules*, *36*, 2049 (2003).
3. G. Liu, X. Yan, S. Duncan. *Macromolecules*, *35*, 9788 (2002).
4. H. Yamakawa, M. Fujii. *Macromolecules*, 7, 128 (1974).
5. H. Yamakawa, T. Yoshizaki. *Macromolecules*, 13, 633 (1980).

IV. Results and discussion

IV-1. Nanofiber solutions in molecular solvents.

We performed Static and Dynamic VV (polarized) and VH (depolarized) Light Scattering experiments on PS-b-PI nanofibers on dilute equilibrated solutions. Static light scattering experiments in dilute solutions gave satisfactory results on size (R_c) and molecular weight per unit length (M_u). We also obtained a quite good approximation of the persistent length (l_p). Dynamic light scattering experiments verified the fact of having long objects and gave us the range of size. Dilute samples gave us our results. Static and Dynamic Light Scattering measurements were carried out in dilute solutions in two different solvents (THF and toluene).

In the static light scattering experiment we measure many angles for a short period of time. This gives us the values of the mean scattered intensity for many different angles. Static VV measurements gave us the ability to get useful information on the cross-section radius, the persistent length and the mass per unit length in the accessible q range. All nanofiber solutions fall in the dilute regime $C \approx 10^{-5}\, g/cm^3$.

The intensities of the nanofibers in both solvents are given as a function of q are given in Figure IV-1. The slope of value -1 is indicative of rodlike behavior.

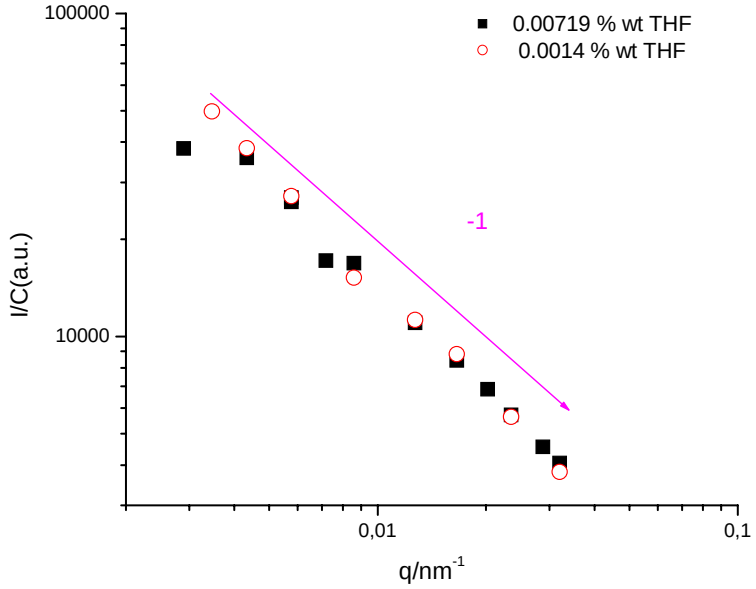

Figure IV-1: A double log-log plot of the reduced intensity versus the logarithm q.

The overall shape of the nanofibers resembles that of a rod, since the I(q) scales approximately with q^{-1}. (solid line in Fig IV-1).

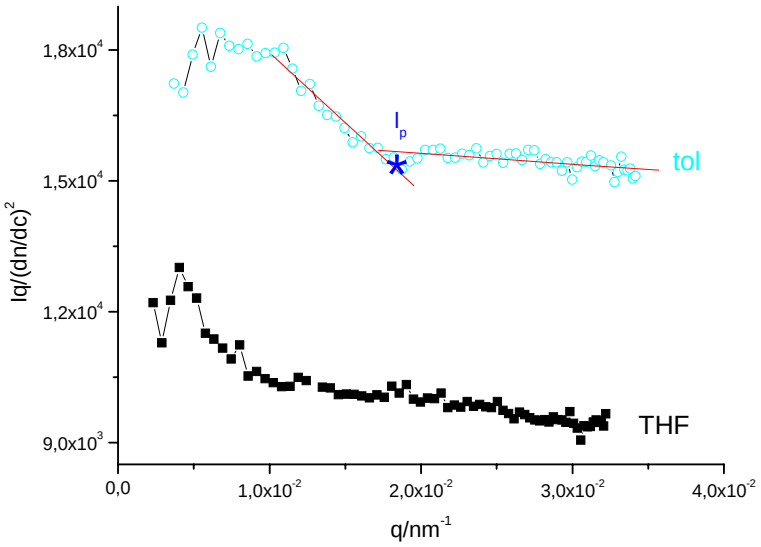

Figure IV-2: A comparison plot between the scattering intensity profiles of the dilute solutions in THF and toluene.

A more sensitive representation of the data shown in Iq versus q is shown in Figure IV-2 for 7.2 10^{-3} % wt in THF and 15.5 10^{-3} %wt in toluene over the whole q range. In fact Iq is not flat which indicates either a structure flexibility of finite diameter. The reduced intensity I/C is normalized to the isotropic intensity of the neat solvent taking into account the difference in the refractive indexes.

For rodlike shapes with core diameter of R_c.

$$qI = (qI)_0 e^{\frac{-R_c^2 q^2}{2}} \qquad \textit{IV-1}$$

A fit of the eq IV-1 to the exponential Iq of Fig IV-2 yield Rc=17nm or d=34nm.

At high $q>q_c$ Iq versus q yields an estimatation of the persistent length (Figure I-6) $lp=2/q_c$; $l_p \approx 200nm$ in THF and 130nm in toluene.

The persistent length is in good agreement with the previous results. From the point where points start to deviate from the slope in figure IV-2, we get the value of the persistent length using the equation. It was calculated to be lp=200nm from the THF data and 127nm from the toluene data.

The value of $Mu=M_w/L$ was derived from: $K^*M_u=q(R_{vv}/C)$ (eq. IV-2). Taking $\lim_{q \to 0} q\frac{R_{VV}}{C} = 1.16 nm^{-1} cm^{-1}$ and using $K^* = \frac{4\pi^2 \tilde{n}_0^2 \left(\frac{d\tilde{n}}{dc}\right)^2}{\lambda_o^4 N} = 3.54 \cdot 10^{-7} cm^2 g^{-2} mol$ and $\frac{d\tilde{n}}{dc} \cong 0.148 cm^3/gr$ we obtained the linear mass density M_u= 22 10^5 g/(mole nm).

Table IV-1 summarizes our findings along with G. Liu's results.

Table IV-1: Characteristics of the PS-b- PI Nanofiber.

Prof G. Liu's data	Our work (dilute THF)	Our work (dilute toluene)
SLS L_w=1770nm	-	-
TEM L_w=1930nm	-	-
L_N=1310nm	-	-
d_{PI}=26.6±1.7nm	34nm	-
$\frac{dn_r}{dc} = 0.148\frac{mL}{g}$		0.08cm^3/gr
M_w=(3.53±0.06) 10^8g/mol	-	-
R_G=443±1nm	-	-
l_p=365±5nm	≈200nm	130nm
M_u=2.00 10^5g/(mol nm)	22 10^5g/(mole nm)	-

Above about C* ≈ M_w/L^3≈ 10^{-5} g/cm^3 the nanofibers will start to interfere. We should mention however that the concept of C* in rodlike polymers does not describe very well their behavior. As we measure concentrations above the calculated C* we observe that we are still in the dilute regime.

IV-2. Dynamic light scattering measurements

The technique probes concentration fluctuations with wavelength 2π/q. For non-interacting particles undergoing translational diffusion, a characteristic time $(q^2 D_o)^{-1}$ is associated with the decay of this particular wavelength. The light scattering intensity therefore fluctuates in time around the average value $|I(q)|$ and the information given from the molecular motion is included in the time correlation function C(q,t) (eq III-1).

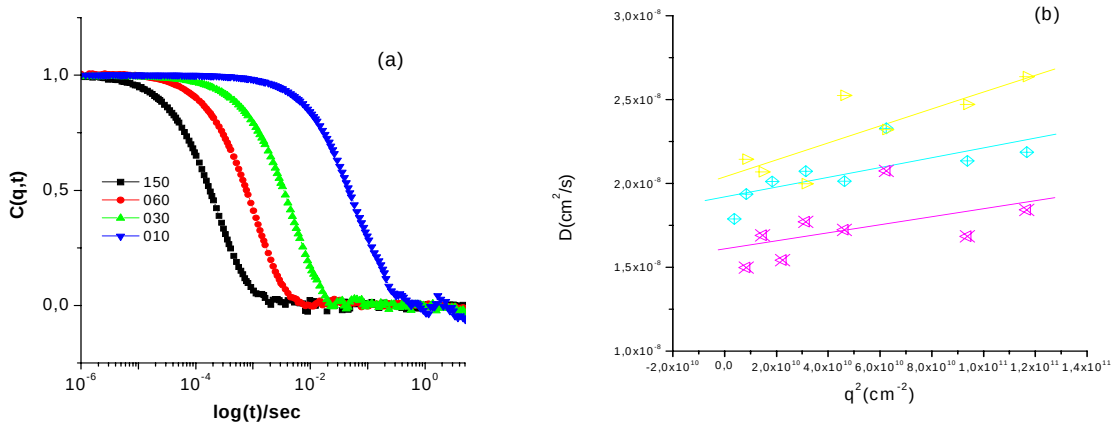

Figure IV-3: The relaxation function for the concentration density fluctuations in dilute THF solution at different scattering angles (a) The diffusion coefficients for the concentrations is shown in (b).

Using the Stokes Einstein relation (equation II-15) and the values of the diffusion coefficient in figure IV-3(b) we obtain 80nm for the hydrodynamic radius. Note the difference between R_h and R_g (table III-1).

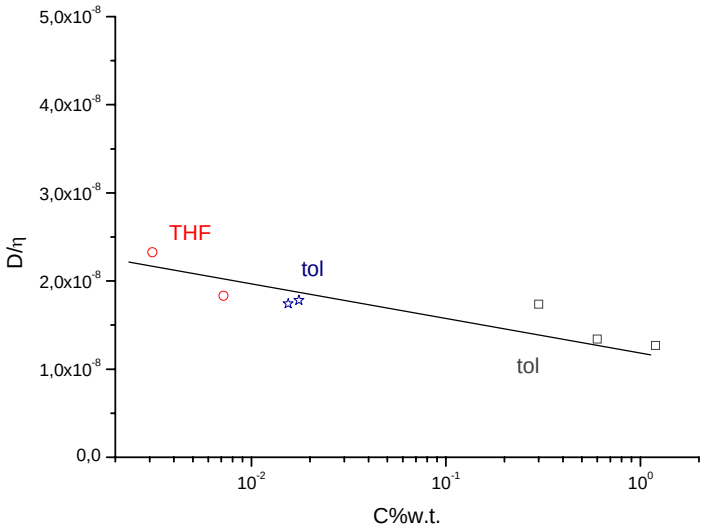

Figure IV-4:Concentration dependence of the diffusion coefficient D for the nanofibers in the two solvents, taking into account the difference in the solvent viscosities.

Taking into account Figure IV-4 and $D=D_o(1+k_DC)$ (equation IV-3) we observe that the slope $k_D<0$ and so is the second Virial coefficient which implies not favorable interactions which could drive to aggregation. Nevertheless up to concentration 1%wt there is no indication of aggregation.

IV-3. Dynamic depolarized light scattering measurements

The scattering of laser light in the depolarized mode (VH) is induced by orientation fluctuations, which cause fluctuation of the anisotropic part of the polarizability tensor. The main origin of the VH intensity is the intrinsic anisotropy of the scatterer (in our case the PS-b-PI nanofibers), which depolarize an incident beam impinging on it. In our case we want to quantify the orientation of the nanofibers in dilute solution.

The correlation functions are good (Figure IV-5).

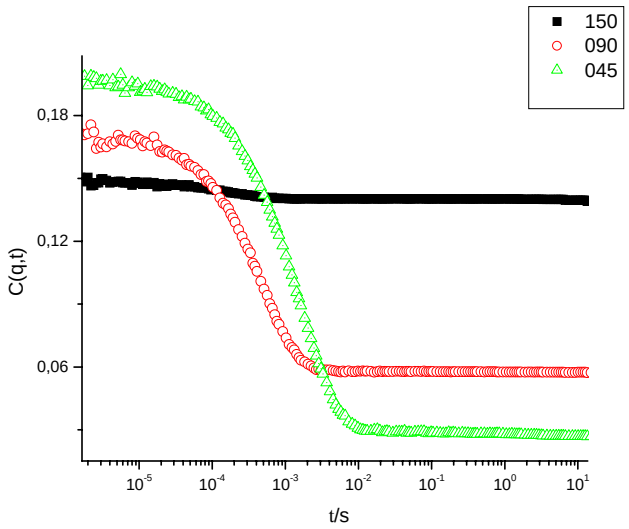

Figure IV-5: The orientation relaxation functions.

In THF we have the double scattering effect, which results in really strong intensities in the correlator. In the toluene solvent we don't have such an effect, that's the reason that we changed solvent from THF to toluene. In toluene the occurrence of double scattering is less, because the refractive index of toluene n is similar to that of the nanofibers. So $\Delta n = n_{nanofibers} - n_{solvent}$ in the case of toluene is reasonably small. In double scattering[1] the intensity is analogous to $(\Delta n)^4$ (equation II-5).

IV-4. Dilute nanofibers in polymeric solvents

Knowing the molecular characteristics of the nanofiber undergoing unrestricted diffusion in liquid dispersions, we examine next their physical state in homopolymer networks. Can the nanofibers move through the network? Does the depletion mechanism drive the nanofibers to aggregate? (figure II-3 and II-4). We recall that the coat of the nanofibers consists of polystyrene. We have therefore selected PS homopolymers been chemically identical to the nanofiber coat. In both cases we vary the concentration of the polystyrene solution, while the nanofiber concentration remains constant at very dilute solution. The concentration range for the low molecular weight polystyrene varies from 2%wt to 60%wt.,while for the high molecular weight ranges from 0.1%wt to 4.4%wt, with estimated C* at 55%wt and 1.3%wt respectively.

IV-4-1. Low molecular weight polystyrene matrix

In this case the polystyrene and the nanofiber's hairs have comparable sizes. For all the examined concentrations in the experimental C(q,t) (figure IV-6) two modes are apparent. After the Inverse Laplace transform we get two peaks. The fast peak is attributed to the polystyrene mode, while the slow peak is due to the nanofibers mode (figure IV-7).

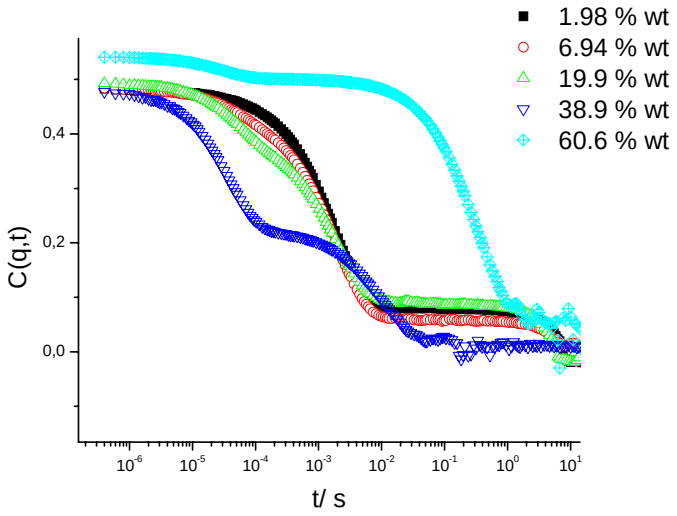

Figure IV-6: Concentration relaxation functions recorded at 45° for different polystyrene concentrations.

Figure IV-6 reveals strong concentration effects on the overall shape of C(q,t). The nature of the two individual processes can be identified by the q dependence of the corresponding rate and intensity. These two quantities are obtained from the C(q,t) (figure IV-7(a)) and the subsequent analysis (equation III-2) via inverse Laplace transform (figure IV-7(b)).

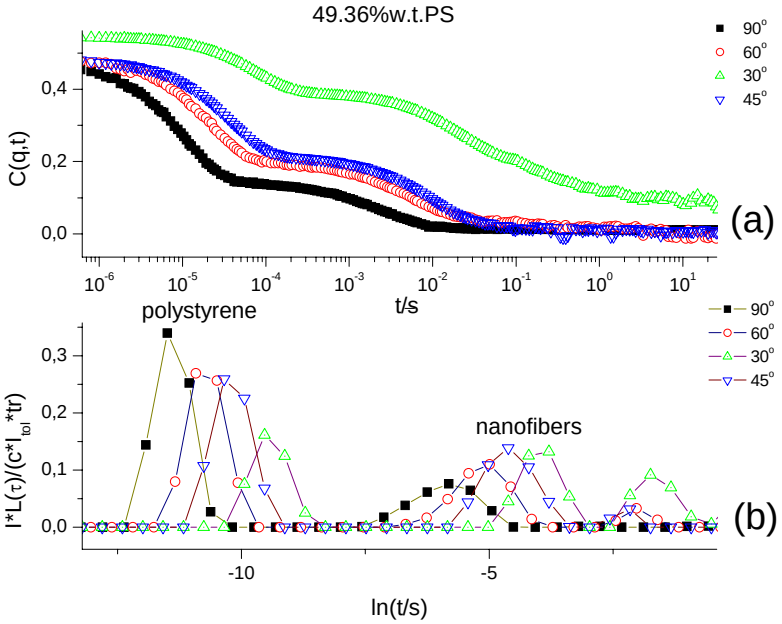

Figure IV-7: The distribution relaxation function (a) when analyzed with the contin according to eq III-2 yield the b) corresponding distribution relaxation function L(lnτ).

The q dependence of the effective diffusion $D=\Gamma/q^2$ (equation IV-4) and the intensity for the fast and the slow processes of C(q,t) are shown in figure IV-8 for a 49%wt concentration in polystyrene and 5.773 10^{-4} %wt in nanofibers. Figure IV-8 (a) represents the intensity versus q for the polystyrene macromolecules in a logarithmic scale in both axes. Figure IV-8 (b) represents the intensity of the nanofibers versus q. The

slope is close to –1 and that is an indication of rodlike behavior as in the dilute suspension (Figure IV-1). Figure IV-8 (c) represents the diffusion coefficient of the polystyrene macromolecules, which is of the order of 10^{-6} cm^2/sec. Figure IV-8 (d) represents the diffusion coefficient of the nanofibers, which is by more than two orders of magnitude slower than the polystyrene solvent. Due to this vastly different dynamics the two modes are uncoupled and can be safely associated to the constituent components of the molecular composite.

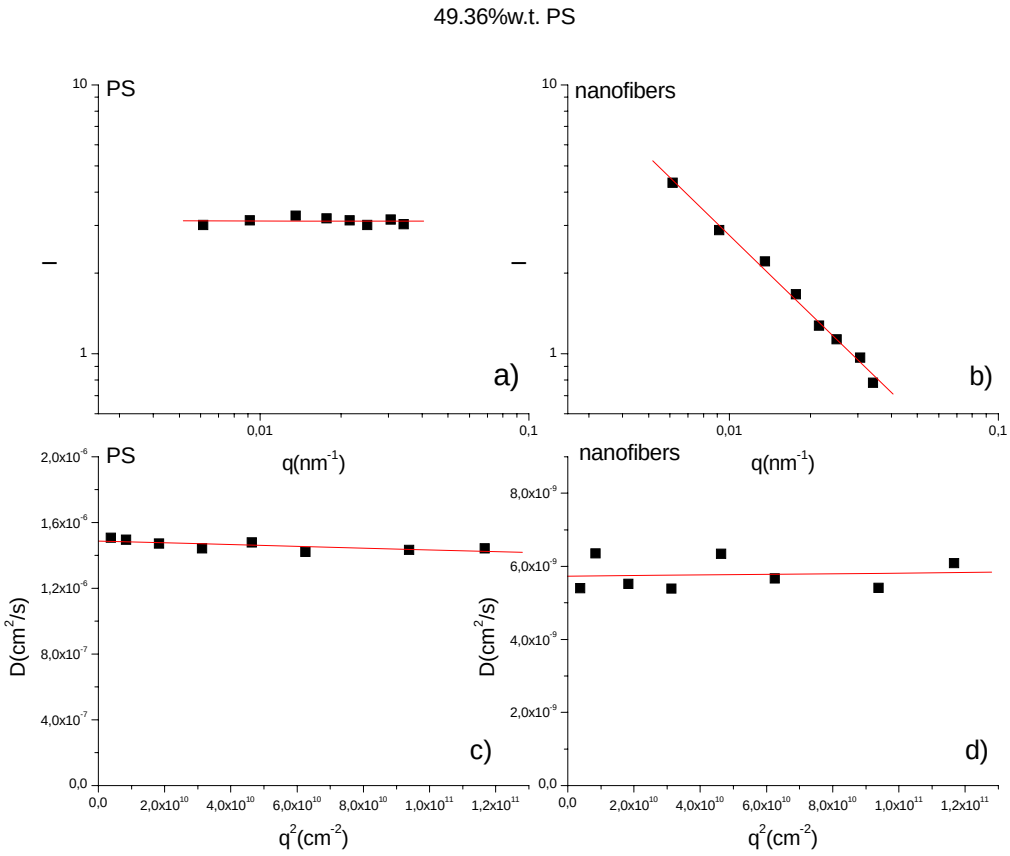

Figure IV-8: Intensity and diffusional rate $\Gamma(q)/q^2$ associated with the processes of figure IV-8 a, c) polystyrene component b, d) nanofibers.

Due to this vastly diffusional dynamics , the two modes are uncoupled and can be safely associated to the constituent components of modules they composite.

The polystyrene chains forming the polymer network, is not affected by the presence of the nanofibers, since the diffusion coefficient has the typical behavior of a homopolymer in a good solvent. As their concentration is increased the density of the network reaches higher and higher values. In the beginning we have dilute polystyrene molecules in the toluene solvent, then we reach the semidilute regime and in the end we have the presence of a dense polymer network.

In figure IV-9 the normalized intensity of the polystyrene solution relative to the concentration value is shown as a function of concentration. The first two points depict the dilute regime values, the next three the overlap regime values and the last point represents the semidilute regime, with observable decrease of the intensity value. The turning point of the function in the second graph when projected on the χ axis represents the C* value. We estimated that C*

$$C^* = \frac{M_w / N_A}{4/3\,\pi R_g^3} \qquad \textit{IV-5}$$

and found a value of 55%wt.

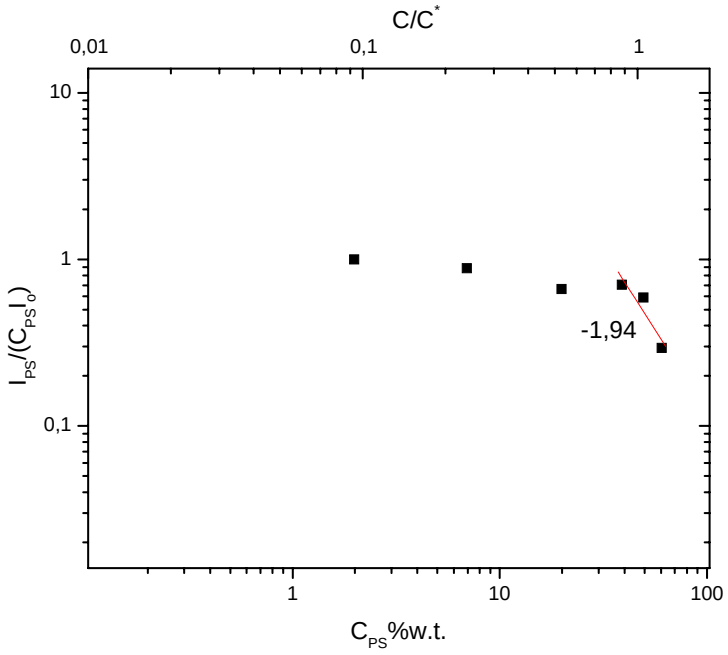

Figure IV-9: The intensity of the fast component normalized to the value for the dilute polystyrene solution. The slope -1.3 denotes scaling law relationship.

The value of the C* already mentioned nearly seems to be a good estimate since it approximately captures the turn over of I(C).

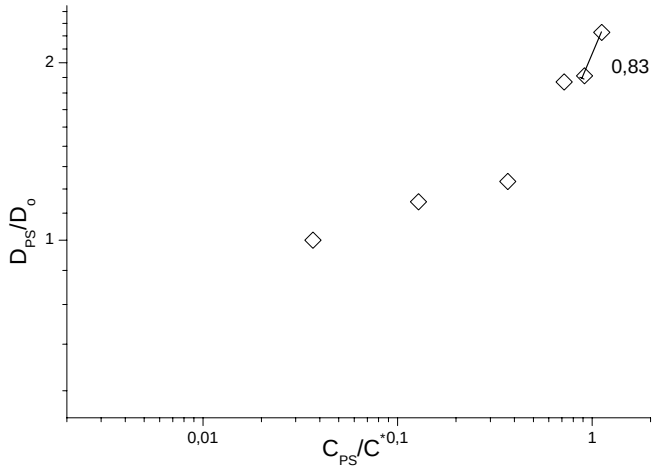

Figure IV-10: Normalized cooperative diffusion D_c/D_o versus reduced concentration C/C*. The slope 0.77 denotes the scaling law relationship.

Figure IV-10 depicts the normalized diffusion coefficient of the polystyrene chains relative to the diffusion coefficient in the dilute regime as a function of the reduced C/C*. However, D/D_o varies stronger with C/C* than forseen for the cooperative diffusion in semidilute solution of homopolymers. This suggests stronger osmotic forces. The latter is corroborated by the Intensity plot of figure IV-11 which indicates stronger decrease of I with C than predicted by the scaling relationship. This might relate to polystyrene homopolymer- polystyrene hairs in the nanofibers interactions in analogy to the multiarm star solutions[2]. The fast process can still be identified with the cooperative diffusion, based on the concentration dependence of the diffusion coefficient and the scattered intensity.

Figure IV-11 presents the intensity dependence of the nanofibers versus q. At $C<C^*$ of the polystyrene $I(q)\sim q^{-1}$ like in the dilute solution. On the contrary above C* in molecular solvents a clearly steeper decrease of I(q) with q is observed. In the concentration 60%wt were also observed two modes for the nanofibers. The first with slope close to -1 indicative of rodlike behavior and the second with slope close two -2 indicative of aggregation. Bigger particles have higher q dependence and the slope is steeper –2 in contrast to the single rodlike particle behavior with slope –1.

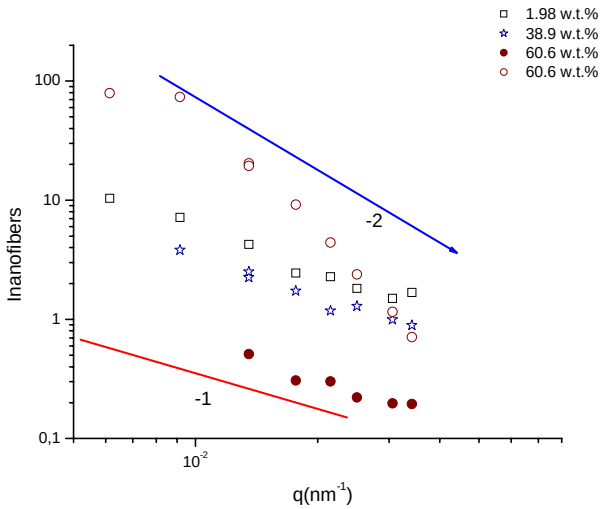

Figure IV-11: The intensity profile I(q) for the nanofibers in the solution at different polystyrene concentration as indicated. At the highest polystyrene concentration (60%wt) there is two nanofiber concentrations indicated by the closed and the open cycles.

The concentration dependence of the slow mode $I_{nanofibers}$ at a given angle 45^{o} is visualized in figure IV-12. The first five points represent rodlike behavior of separate and not aggregated nanofibers, while the last point's value skyrockets and is representative of aggregated particles. The point with the star symbol coexists in the same solution with the aggregated nanofibers and represents a fraction of nanofibers that is not aggregated. A rough estimation of the non aggregated fraction is the ratio of their intensities relative to the average value of the intensity five slower concentrations. The much higher intensity associated with the supramolecular nanofibers aggregates is due to its larger size. This solution state, the diffusion coefficient should map these two species. In fact, figure IV-13 signals the onset of the slow down of the single nanofiber at C close to the C^{*} and provides an estimate value of the induced aggregation from the disparity of the two D's at $C \approx 2C^{*}$.

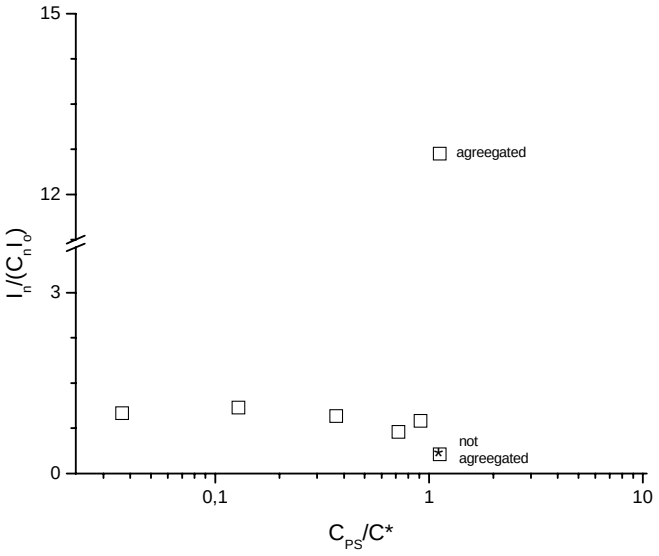

Figure IV-12: The normalized intensity versus the reduced concentration at 45^o.

Figure IV-13 depicts the normalized diffusion coefficient of the nanofibers. After the first three points we observe a decrease of the diffusion coefficient value. We have single particles that move slower because of the presence of the network. The last point, which represents the aggregated nanofibers, moves really slow because the particles are bigger.

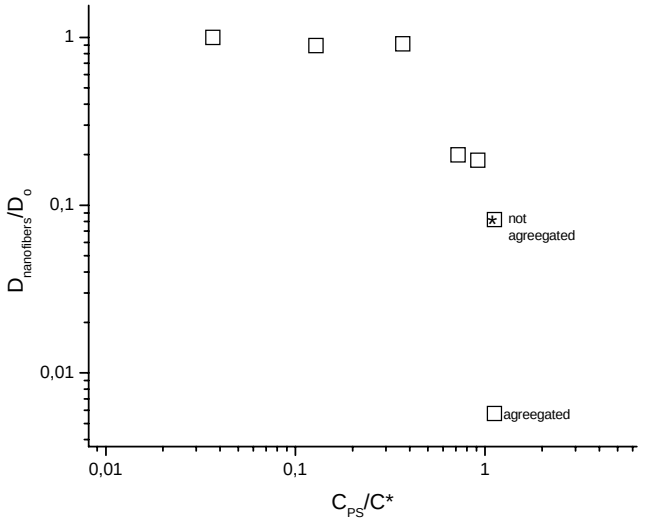

Figure IV-13: The diffusion coefficient of the nanofibers as a function of the reduced C/C* normalized to the corresponding concentration value at C→0.

IV-4-2. High molecular weight polystyrene matrix

In the nanofiber plus short polystyrene system the nanofibers form supramolecular assemblies above about C*. Owing to the low molecular mass of the polystyrene, the C* value is very high so that the semidilute regime is restricted. We have therefore complemented this investigation by using the very high molar mass polystyrene-nanofiber system.

Due to the stronger scattering intensity of this high molar mass polystyrene, the contribution of the nanofiber becomes evident at C>C* compared to the low molar mass polystyrene-nanofiber systems. The analysis of the two processes proceeds like for the latter system namely by assigning the q dependence of the intensity and rate of the two components of C(q,t) in figure IV-14.

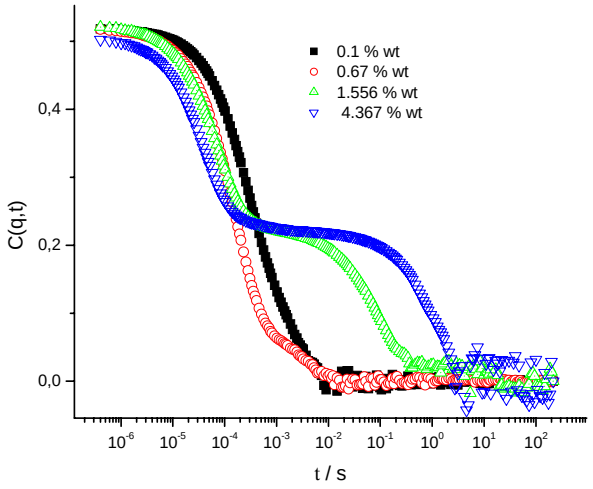

Figure IV-14: Relaxation functions in dilute nanofiber-polystyrene solutions for different polystyrene concentrations at $\theta=60^{o}$.

The relaxation functions of figure IV-15 (a) depict the evolution of the fast (polystyrene component) and the slow (nanofibers) processes with scattered angle. Inverse Laplace transform, based on the two present peaks gives figure IV-15 (b). The corresponding intensities and diffusive rates are shown as a function of q in figure IV-16 for the system with 1.55%wt polystyrene (~2C*) and 3.13 10^{-4} % wt nanofibers.

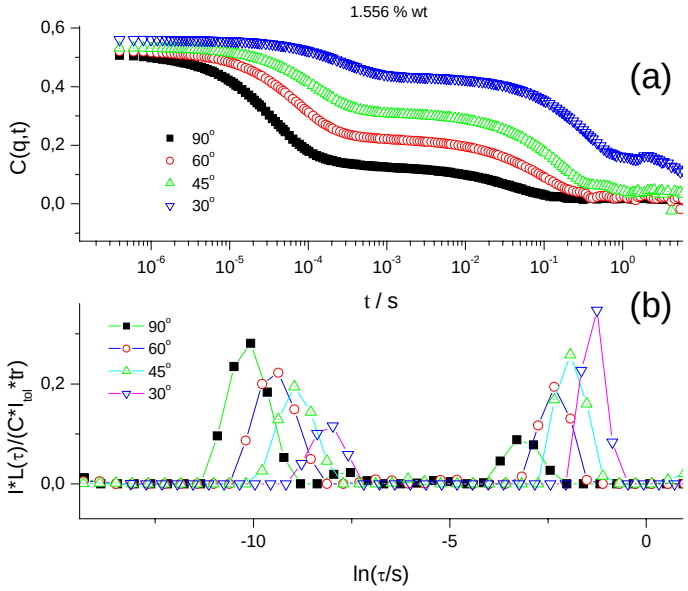

Figure IV-15: Relaxation functions (a) along with the distribution of relaxation times (b) 1.55% wt PS in toluene with 3.13 10^{-4} % wt nanofibers at four different scattering angles.

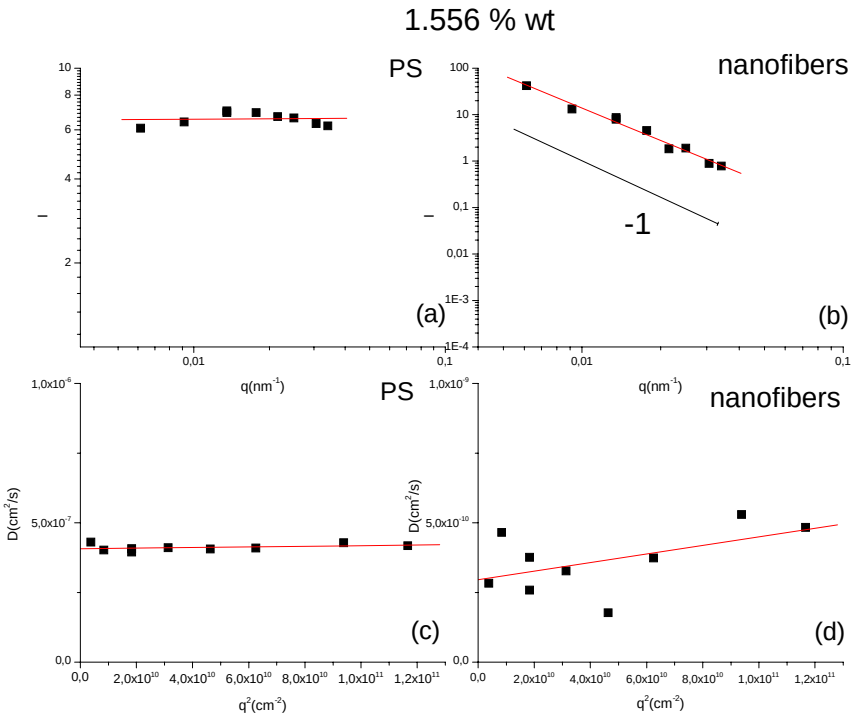

Figure IV-16: a) Intensity and diffusion constant for the fast (polystyrene component, left panel) and the slow (nanofibers, right panel) of the 1.55 %wt polystyrene-nanofiber as a function of q. The I(q) of the slow component is steeper than I(q)~q^{-1}(solid line in figure IV-16(b)).

On the q dependence of the data in the left panel of figure IV-17 with very weak q dependant intensity and D=4 10^{-7} cm^2/s is based the assignment of the fast process to the cooperative diffusion of the polystyrene network at C≈2C*. Alternatively the strong I(q) and the low D=3 10^{-10} cm^2/s of the right panel in figure IV-17 are comparable with the association of the slow process to the nanofibers. The variation of these quantities with concentration is depicted in figure IV-18 for a constant q=0,01768nm^{-1} (θ=60°).

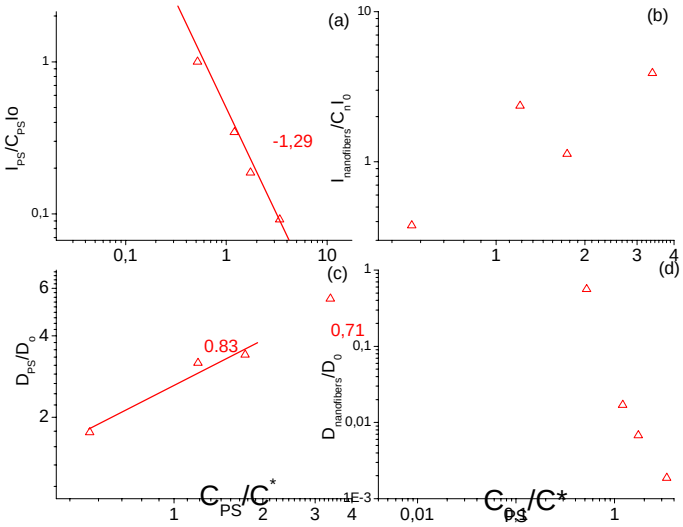

Figure IV-17: a) The intensity (normalized to the corresponding value at C⟶0) and the diffusion (normalized to D(C=0) of the fast polystyrene (right panel) and the slow nanofibers (left panel) at a given q= 0,01353nm^{-1} (θ=45°).

The concentration dependence of fast process characteristics (left panel of figure IV-17) confirms a typical, unperturbed, from the presence of nanofibers, behavior of a semidilute solution of homopolymers above C* estimated to be about 1.3%wt (I_{PS} and D_{PS} conform to the scaling relations (solid lines). The slowing down of the D_{nanof} results from the increase of the solution viscosity.

The figure IV-18 presents the intensity of the nanofibers versus q. Note that the nanofibers have the same dilute composition in all examined solutions. At the lowest polystyrene concentration, $I(q)\sim q^{-1}$ like in dilute nanofiber suspensions (figure IV-1) while I(q) becomes steeper at higher polystyrene concentrations. The latter finding strongly suggests formation of supramolecular nanofiber assemblies.

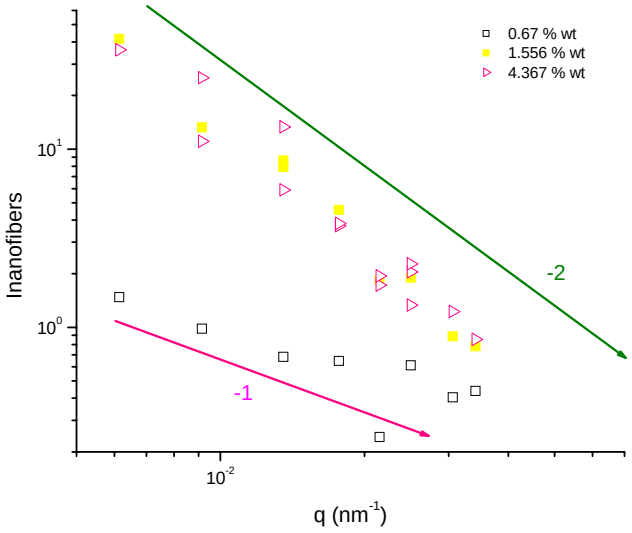

Figure IV-18: The intensity profile I(q) for the dilute nanofibers at different polystyrene concentrations indicated in the plot.

IV-4-3. Comparison of the nanofibers state in polymer matrices

A compilation of the data characterizing the nanofiber state in the two polystyrene matrixes is presented in the next section.

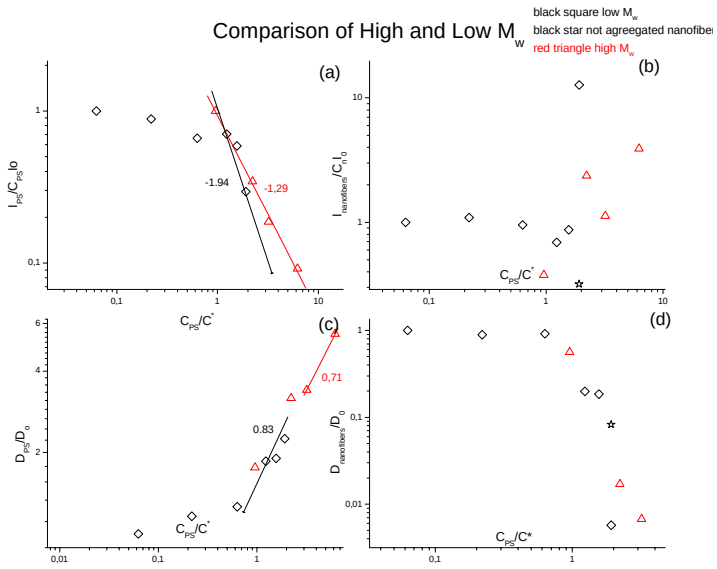

Figure IV-19: The intensity and the diffusion (normalized to the corresponding values at C=0) of the fast (polystyrene) and the slow (nanofibers) at a given q for the two polystyrene-nanofiber systems.

We have used the fast (polystyrene) process as an internal calibration for the C*. We have therefore adjusted C* for the high molar mass polystyrene to 0.7% wt to have a superimposed I_{PS} and D_{PS} for the two polystyrenes. Overall the picture resembles well semidilute solutions of linear homopolymers in a good solvent (see slopes in figures IV-

19 (a) and (c)) suggesting negligible interactions with the nanofibers. The latter on the contrary form aggregates above the overlap concentration C* as indicated by the strong increase of their intensity. The value of the increased viscosity on the slowing down of D_{nanof} with concentration beyond C* (figure IV-19 (d)) is therefore partly due to the increased size of the nanofibers. The appearance of aggregation roughly above C* is in account to the depletion mechanism also discussed by Dogic et al[3]. The value of the increased viscosity on the slowing down of D_{nanof} above C* is certainly important and is estimated below.

The viscosity of the polystyrene solutions was estimated from the data at similar polystyrene molar masses reported by Phillies and Peczak[4]. The normalized η_s (to the solvent viscosity) interpolated by our polystyrene is plotted as a function of concentration in figure IV-20. Using these data we have accounted for the viscosity effect on D in the plot D_η in figure IV-21.

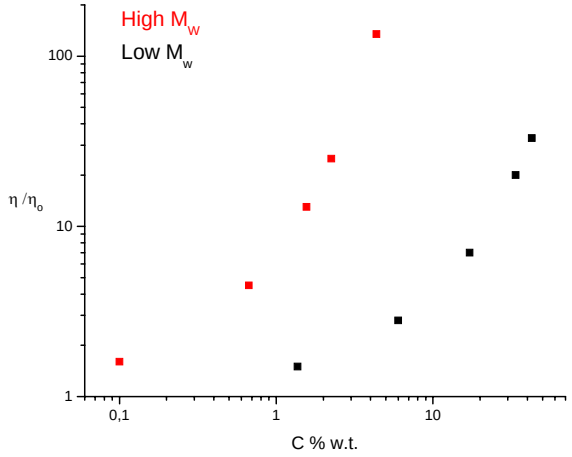

Figure IV-20: The normalized viscosity (to the solvent viscosity) of polystyrene solutions for the two molar masses used in this study.

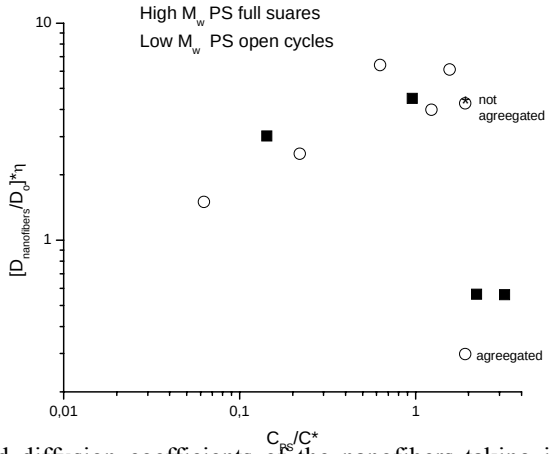

Figure IV-21: Normalized diffusion coefficients of the nanofibers taking into account the effect of the solution in the two polystyrene nanofiber systems.

Given the interpolation errors in figure IV-20, the data of figure IV-21 clearly support the aggregation above C* since D_η decreases for C>C*. Therefore, the formation of aggregated nanofibers is supported by both the intensity and the diffusion data of nanofibers, whose contribution can be resolved only from the present dynamic light scattering experiment.

References

1 G. Fytas, D. Vlassopoulos, G. Meier, A. Lichtmann and A.N.Semenov. *Phys. Rev. Lett.*, 76, 3586 (1996).

2 A.N. Semenov et al. *Langmuir*, 15, 358 (1999).

3 Z. Dogic, K. Purdy, E. Grelet, M. Adams, S. Fraden. *Phys. Rev. E*, 69, 051702 (2004).

4 G.D.J. Phillies and Pavel Peczak. *Macromolecules*, 21, 214, (1988).

V. Conclusions

Diblock copolymer chemistry allows the production of particles with designed persistent shape. In particular long cylindrical particles can be obtained by crosslinking a polyisoprene cylinder with polystyrene chains (M_w=7k) forming the coat. The supramolecular structure, with core diameter d_{PI}=26.6nm and cylinder length L_w=1930nm can be isolated. Such a sample was synthesized and characterized from the laboratory of Prof. G. Liu in Calgary since the precursor diblock copolymer is the polystyrene-b-polyisoprene. We call the resulted assembly the PS-b-PI nanofiber. It is a diblock copolymer nanofiber consisting of crosslinked cylindrical core made of one block (polyisoprene) and surface anchored chains made of another block (polystyrene).

We characterize the nanofibers in dilute equilibrated solutions with static and dynamic light scattering experiments. Dilute static light scattering experiments gave satisfactory results on size R_c and molecular weight per unit length M_u. We also obtained a quite good approximation of the persistent length l_p, and verified a rod like overall shape from the profile of the scattering intensity. Dynamic light scattering experiments yielded a rather low value for the hydrodynamic radius compatible with the anisotropic shape of the nanofibers.

In order to get an insight of the structure and diffusion of this long fibers in a chemically identical network of polystyrene homopolymers reflecting their adaptation as fillers, we have studied the physical state of these fibers in polystyrene solution for two molecular weights (M_{w1}=22.2kDa and M_{w2}=1.200kDa). Utilizing photon correlation spectroscopy two processes are clearly observed and unambiguously resolved. These were then attributed to the homopolymer and the nanofiber due to the vastly different inherent dynamics of the components of this molecular composite. At sufficienly low polystyrene concentrations a single particle's behavior is observed, whereas for concentrations above the overlap polystyrene concentration C*, when a transient network is formed, nanofibers tend to aggregate. This was clearly witnessed by the intensity increase and the slowing down of the nanofibers diffusion. The interactions leading to the aggregation probably arise from an unbalanced osmotic pressure due to the exluded volume driven expulsion of polymers from the region between the particles. A depletion mechanism induces aggregation in concentrations greater than C*in both the low and the high molecular weight polystyrene in a good solvent cases.

Appendix

A-1. Kinetics

The question that arises is whether the measurements were at equilibrium. To investigate such the equilibrium kinetics of our samples we measured a specific sample as a function of time. We investigated the behavior of the nanofibers in a polystyrene solution of molecular weight 1,210,700. The concentration of the polystyrene is in the semidilute regime (2%w.t.), while that of the nanofibers is in the dilute regime.

The good correlation functions (Figure A-1a) were analyzed with the Contin program (figure A-1b).

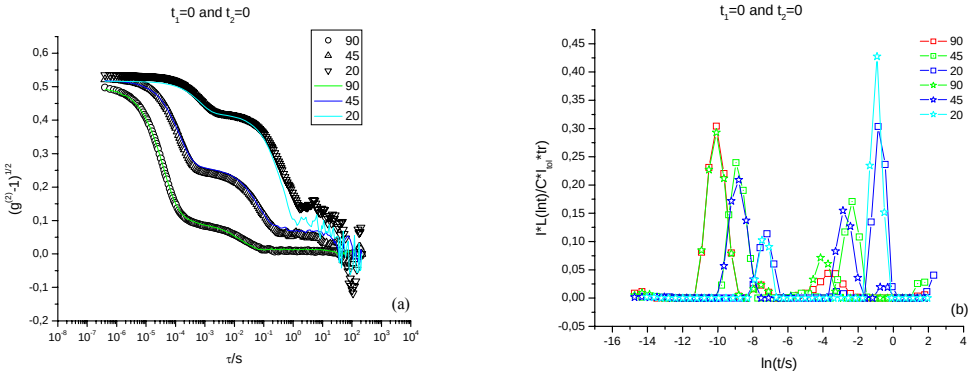

Figure A-1:a) The correlation functions of our sample after (black lines) and before (colored lines) the shaking. b) The correlation functions after the Inverse Laplace transform

We observe a small change in the intensity and the diffusion coefficient of the nanofibers. (Figure A-2b, Figure A-3b). We measure until the sample equilibrates. Small aggregates appear. Then we shake the sample and measure again. We observe that the behavior of the sample is exactly the same as our first measurement. This implies that weak bonds arise among the nanofibers that break down very easily. These small agreegates disappear and we have the exact behavior that we had before.

The increase of slope and the total increase of the intensity at low q indicates an increased size and mass of the scattering particles (figure A-2b). This could be induced through aggregation of few nanofibers together driven by the depletion mechanism. Such an aggregation is somewhat confirmed by the small measurable decrease of the diffusion coefficient. The diffusion coefficients of the polystyrene solutions have no measurable changes.

We conclude that the measurements we have are trustworthy because the samples we measured were equilibrated.

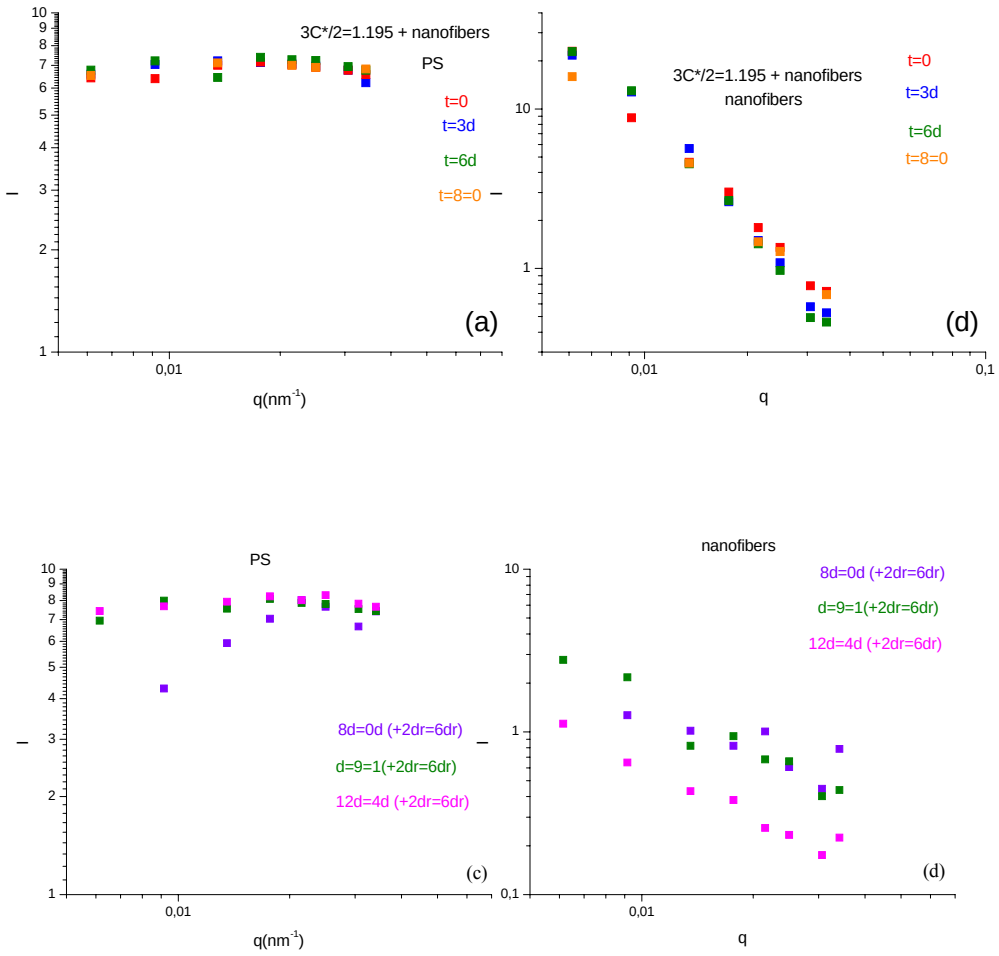

Figure A-2: The intensity of the samples in relation to the scattering factor q, for the a) for the polystyrene mode (in solution of polystyrene and nanofibers) before the shaking t=8=0 days. b) for the nanofibers mode in solution before the shaking, c) for the polystyrene mode in solution after the shaking, d) for the nanofibers mode in solution after the shaking.

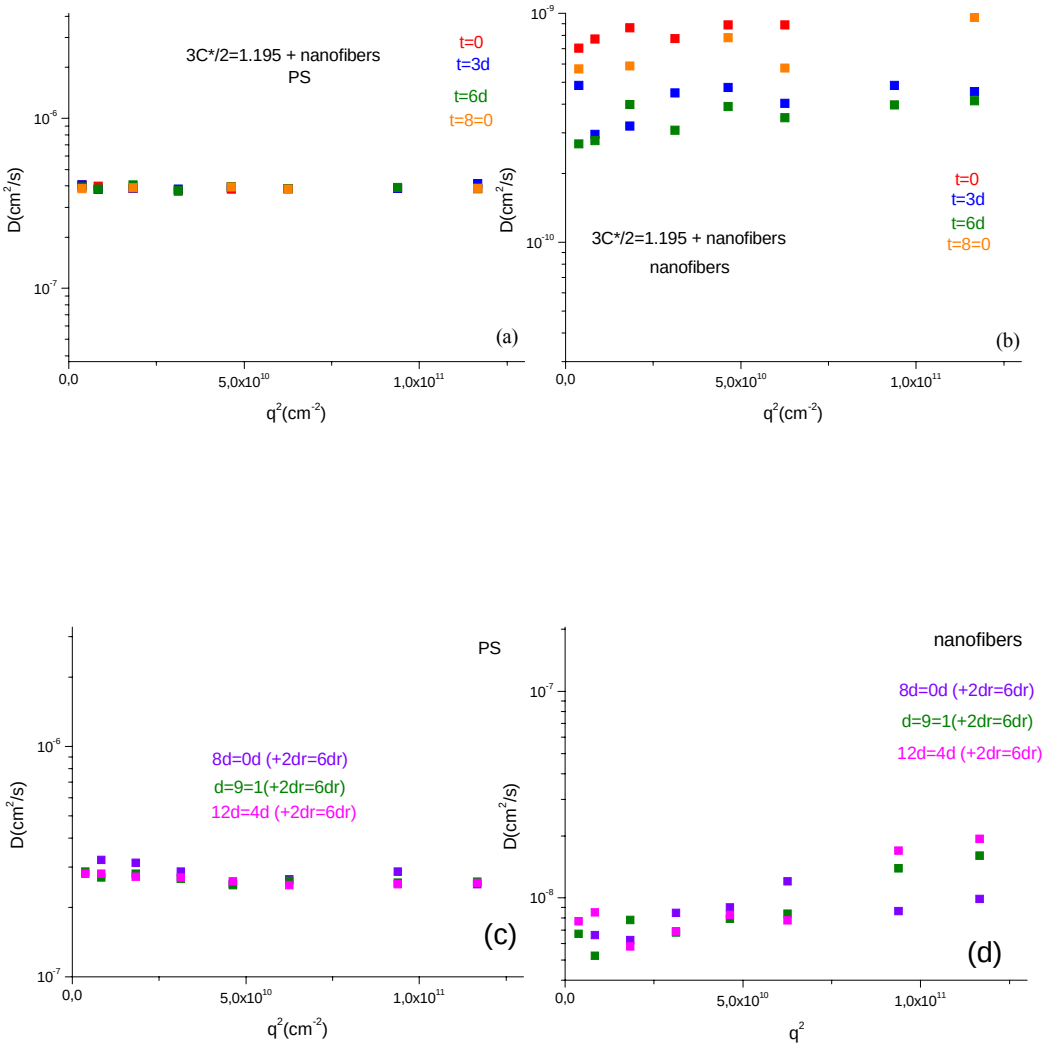

Figure A-3: Diffusion coefficients versus the square of the scattering term, for the a) for the polystyrene mode (in solution of polystyrene and nanofibers) before the shaking t=8=0 days. b) for the nanofibers mode in solution before the shaking, c) for the polystyrene mode in solution after the shaking, d) for the nanofibers mode in solution after the shaking.